Journal of South American Earth Sciences 29 (2010) 105–127

Contents lists available at ScienceDirect

Journal of South American Earth Sciences

journal homepage: www.elsevier.com/locate/jsames

The Western Sierras Pampeanas: Protracted Grenville-age history (1330–1030 Ma) of intra-oceanic arcs, subduction–accretion at continental-edge and AMCG intraplate magmatism

C.W. Rapela [a,*], R.J. Pankhurst [b], C. Casquet [c], E. Baldo [d], C. Galindo [c], C.M. Fanning [e], J.M. Dahlquist [d]

[a] Centro de Investigaciones Geológicas, Universidad Nacional de La Plata-CONICET, 1900 La Plata, Argentina
[b] British Geological Survey, Keyworth, Nottingham NG12 5GG, United Kingdom
[c] Departamento de Petrología y Geoquímica, Universidad Complutense, 28040 Madrid, Spain
[d] Departamento de Geología, Universidad Nacional de Córdoba, 5000 Córdoba, Argentina
[e] Research School of Earth Sciences, The Australian National University, Canberra, Australia

ARTICLE INFO

Article history:
Received 9 February 2009
Accepted 5 August 2009

Keywords:
Sierras Pampeanas
Grenville-age orogeny
Intra-oceanic arc
Arc–continent collision
AMCG complex
U–Pb SHRIMP dating

ABSTRACT

New U–Pb SHRIMP zircon ages combined with geochemical and isotope investigation in the Sierra de Maz and Sierra de Pie de Palo and a xenolith of the Precordillera basement (Ullún), provides insight into the identification of major Grenville-age tectonomagmatic events and their timing in the Western Sierras Pampeanas. The study reveals two contrasting scenarios that evolved separately during the 300 Ma long history: Sierra de Maz, which was always part of a continental crust, and the juvenile oceanic arc and back-arc sector of Sierra de Pie de Palo and Ullún. The oldest rocks are the Andino-type granitic orthogneisses of Sierra de Maz (1330–1260 Ma) and associated subalkaline basic rocks, that were part of an active continental margin developed in a Paleoproterozoic crust. Amphibolite facies metamorphism affected the orthogneisses at ca. 1175 Ma, while granulite facies was attained in neighbouring meta-sediments and basic granulites. Interruption of continental-edge magmatism and high-grade metamorphism is interpreted as related to an arc–continental collision dated by zircon overgrowths at 1170–1230 Ma. The next event consisted of massif-type anorthosites and related meta-jotunites, meta-mangerites (1092 ± 6 Ma) and meta-granites (1086 ± 10 Ma) that define an AMCG complex in Sierra de Maz. The emplacement of these mantle-derived magmas during an extensional episode produced a widespread thermal overprint at ca. 1095 Ma in neighbouring country rocks. In constrast, juvenile oceanic arc and back-arc complexes dominated the Sierra de Pie de Palo–Ullún sector, that was fully developed *ca.* 1200 Ma (1196 ± 8 Ma metagabbro). A new episode of oceanic arc magmatism at ~1165 Ma was roughly coeval with the amphibolite high-grade metamorphism of Sierra de Maz, indicating that these two sectors underwent independent geodynamic scenarios at this age. Two more episodes of arc subduction are registered in the Pie de Palo–Ullún sector: (i) 1110 ± 10 Ma orthogneisses and basic amphibolites with geochemical fingerprints of emplacement in a more mature crust, and (ii) a 1027 ± 17 Ma TTG juvenile suite, which is the youngest Grenville-age magmatic event registered in the Western Sierras Pampeanas. The geodynamic history in both study areas reveals a complex orogenic evolution, dominated by convergent tectonics and accretion of juvenile oceanic arcs to the continent.

1. Introduction

In the 26–33°S flat-slab segment of the Nazca plate in the Southern Andes, present-day landforms result from basement uplift on Miocene-to-Recent reverse faults located up to 900 km away from the trench. These basement exposures of the Sierras Pampeanas give a unique opportunity to test models of lateral accretion of the continent, from the 2.0–2.2 Ga Paleoproterozoic sequences of the Río de la Plata craton in the east, to the modern Andes in the west (Fig. 1). Based on lithological differences, Caminos (1979) was the first to recognize an eastern group of sierras dominated by abundant Paleozoic granites and metasedimentary rocks (the Eastern Sierras Pampeanas), and a western group characterized by abundant meta-basic, ultrabasic and calc-silicate rocks (the Western Sierras Pampeanas). Modern geochronological studies have demonstrated that the Western Sierras Pampeanas (WSP) preserve a completely different geological history, involving an exposed Mesoproterozoic crystalline basement (e.g., McDonough

* Corresponding author. Fax: +54 221 4827560.
E-mail addresses: crapela@cig.museo.unlp.edu.ar, crapela@way.com.ar (C.W. Rapela).

0895-9811/$ - see front matter © 2009 Elsevier Ltd. All rights reserved.
doi:10.1016/j.jsames.2009.08.004

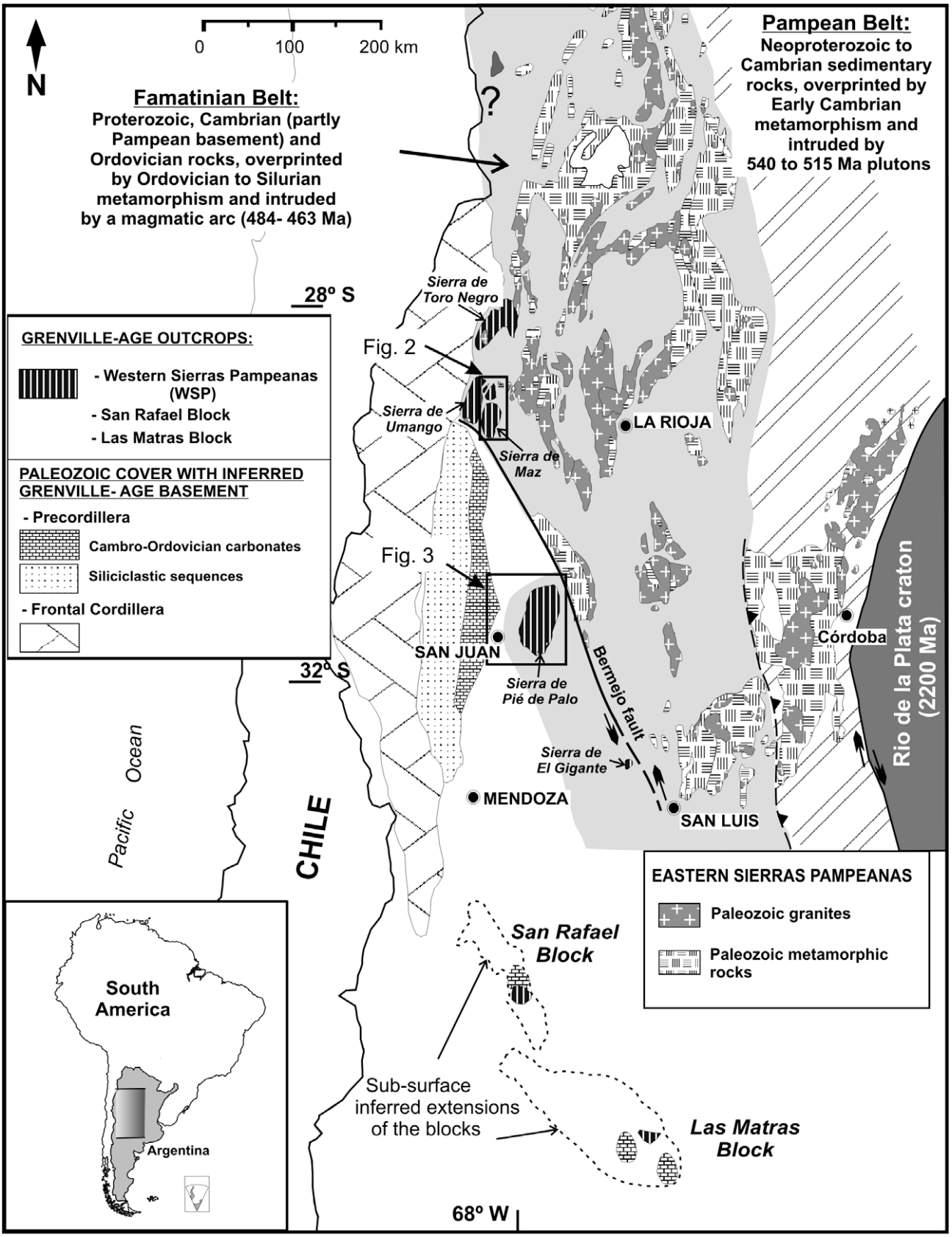

Fig. 1. Location of Grenville-age rock exposures in southwestern South America as well as large Paleozoic units with inferred Mesoproterozoic basement. The outline of the San Rafael and Las Matras blocks are after Sato et al. (2000).

et al., 1993; Pankhurst and Rapela, 1998; Varela et al., 2003; Casquet et al., 2001, 2004; Vujovich et al., 2004). From north to south, the main sierras of the WSP are Toro Negro, Umango, Espinal, Maz, Pie de Palo and El Gigante (Fig. 1). Mesoproterozoic ages have been

also reported to the south of the WSP, in low-relief outcrops of the San Rafael block at 35°S (Astini et al., 1996; Cingolani and Varela, 1999) and scattered outcrops of tonalite–trondhjemites in the Las Matras block at 36° 46′S (Sato et al., 2000, 2004) (Fig. 1). To the west of the WSP, the basement of the Early Paleozoic sequences of the Precordillera is inferred to be Mesoproterozoic in age, based on studies of xenoliths in tertiary volcanic rocks (Abruzzi et al., 1993; Kay et al., 1996), while geochronological data obtained from scattered outcrops of the basement in the Late Paleozoic Frontal Cordillera show that the Grenville-age basement extends further west (Ramos and Basei, 1997; Basei et al., 1998) (Fig. 1). Therefore, a large sector of the Southern Andes basement and foreland, at least 1100 km long, is formed by Grenville-age blocks whose relationships to each other are largely unknown.

The aim of this paper is to start unravelling the early history of this collage of continental blocks by means of a comparative study of the chemistry, isotopic composition, and magmatic-metamorphic history of Sierra de Maz and Sierra de Pie de Palo, two of the largest and best exposed units of the WSP. As in any geological study of the WSP, ours is hampered by a number of uncertainties derived from the numerous rifting and orogenic events overprinted on the Grenville-age basement. Some of the detected overprinting events include: (a) rifting episodes recorded by intrusion of A-type granites at 840 and 770 Ma (Baldo et al., 2006, 2008), and carbonatites and nepheline syenites at 570 Ma (Casquet et al., 2008), (b) Early Paleozoic metamorphism associated with the docking/collision/strike-slip displacement of the WSP and the Precordillera terrane during their final attachment to Gondwana (this has been the topic of much debate in recent years, and reviews have been reported in a special symposium of the 33rd IGC (Casquet et al., 2008; Finney, 2008; Thomas and Astini, 2008), and (c) deformation related to the Late Paleozoic (Gondwanan) and Andean orogenies. The effect of the important Late Paleozoic deformation on the basement is poorly known, whereas the Tertiary–Recent block uplift on reverse faults and imbrication have been better studied. As a result of the Early Paleozoic and Andean tectonics, Grenville-age blocks are imbricated with post-Grenvillian terranes (Casquet et al., 2008), and very detailed studies are needed to establish connections between even adjacent lithological domains.

2. Geological setting

2.1. Sierra de Maz

In the basement of the sierras of Maz and Espinal three domains, separated by first-order shear zones and younger faults (Fig. 2), can be distinguished on the basis of field, geochronology and isotope composition evidence (Casquet et al., 2006; 2008 and references therein). The Eastern Domain consists for the most part of high-grade rocks younger than 1.0 Ga (garnet–sillimanite migmatites and paragneisses with subordinate marbles and amphibolites). Metamorphism took place during the Famatinian orogeny at ca. 440 Ma (see also Lucassen and Becchio, 2003). The Central Domain (also known as the Maz Domain) consists of medium-grade meta-sediments (kyanite–sillimanite–garnet–staurolite schists, quartzites, amphibolites and marbles) and high-grade ultramafic to intermediate meta-igneous and metasedimentary rocks that underwent a Grenville-age orogeny starting at ca. 1.2 Ga (Porcher et al., 2004; Casquet et al., 2006). Deposition of the sedimentary protolith sequences occurred during the Paleoproterozoic (between 1.7 and 1.9 Ga, U–Pb SHRIMP age of detrital zircon, Casquet et al., 2006). Massif-type meta-anorthosites and associated meta-jotunite dykes of 1070 ± 41 Ma are restricted to the eastern side of the Central Domain and show evidence for Famatinian metamorphic rejuvenation at 431 ± 40 Ma (observed throughout the domain, Casquet et al., 2004). Moreover, metamorphic and geochronological discontinuities within the Maz Domain suggest that it is in fact composed of a number of slivers separated by shear zones. All the samples analysed in this study are from the Maz Central Domain (Fig. 2). The Western Domain consists again of metasedimentary rocks younger than 1.0 Ga that underwent Famatinian metamorphism. One sequence of rocks composed of thick marble beds, calcic pelitic schists and quartzites is probably equivalent to the Neoproterozoic Difunta Correa metasedimentary sequence of Sierra de Pie de Palo, and to isotopically-similar rocks of Sierra de Umango (Varela et al., 2001; Galindo et al., 2004). Most rocks within this domain are low- to medium-grade, but high-grade rocks are found locally.

Mylonitic A-type orthogneisses of 840 Ma have been recently reported in the Maz Central Domain and Sierra de Espinal (Baldo et al., 2008), while ca. 570 Ma carbonatites and associated Ne-syenites probably represent the latest rifting event of the Grenville-age block before amalgamation to Gondwana (Casquet et al., 2008).

2.2. Sierra de Pie de Palo

Sierra de Pie de Palo exposes a meta-igneous and metasedimentary complex of stacked nappes thrust towards the west during the Early Paleozoic (Fig. 3). The nappes rest upon the almost unmetamorphosed Precordillera passive-margin sequence of early Cambrian age (Caucete Group), below the Pirquitas basal thrust (Galindo et al., 2004; Ramos et al., 1996; Mulcahy et al., 2007) (Fig. 3).

Grenvillian ages from Sierra de Pie de Palo first reported by Varela and Dalla Salda (1993), McDonough et al. (1993) and Pankhurst and Rapela (1998) were later confirmed in other studies (e.g., Casquet et al., 2001; Vujovich et al., 2004). Two domains with well-constrained Mesoproterozoic lithologies are recognized. A structurally lower unit of mostly meta-mafic and meta-ultramafic rocks composed of serpentinite and metapyroxenite bodies, massive metagabbros, metadiorites, mafic schists, amphibolites and garnet–amphibolites (Vujovich and Kay, 1998 and references therein). This unit is referred to in the geological map (Fig. 3) as the Grenvillian "oceanic arc back-arc complex" (see below). It overlies the siliciclastic and carbonate platform sequences of the Early Paleozoic Caucete Group along the Pirquitas thrust (Vujovich and Kay, 1998) (Fig. 3). An upper imbricate thrust sequence of marbles, calc-silicate rocks, schists, gneisses, quartzites, subordinate amphibolites and abundant acidic orthogneisses, including meta-trondhjemites and meta-tonalites, dominate the central and eastern part of the sierra (Fig. 3). Isotope studies and detrital zircon ages obtained from marbles, calc–silicate schists, quarztites and amphibole–garnet schists in the southern part of the sierra, previously considered Mesoproterozoic, indicate that these rocks in fact constitute a distinct Neoproterozoic platform sequence, the Difunta Correa sequence (580–620 Ma, Galindo et al., 2004; Rapela et al., 2005), which overlies Mesoproterozoic basement. A-type granitic orthogneisses dated at 870 Ma (Baldo et al., 2006), the Difunta Correa metasedimentary sequence and the Mesoproterozoic basement are thoroughly imbricated in the central and eastern part of the sierra. Although a detailed knowledge of the Mesoproterozoic basement in the upper imbricate thrust sequence is still missing, but the assembled lithological includes different types of amphibolites, orthogneisses and metasedimentary rocks. Determination of stratigraphical relationships is however hampered by the strong deformation and difficult access. Intrusion of Early Ordovician granites (470–481 Ma, Pankhurst and Rapela, 1998; Baldo et al., 2005) and Middle Ordovician amphibolite facies metamorphism (455–460 Ma, Casquet et al., 2001; Vujovich et al., 2004) are among the later events registered in Pie de Palo.

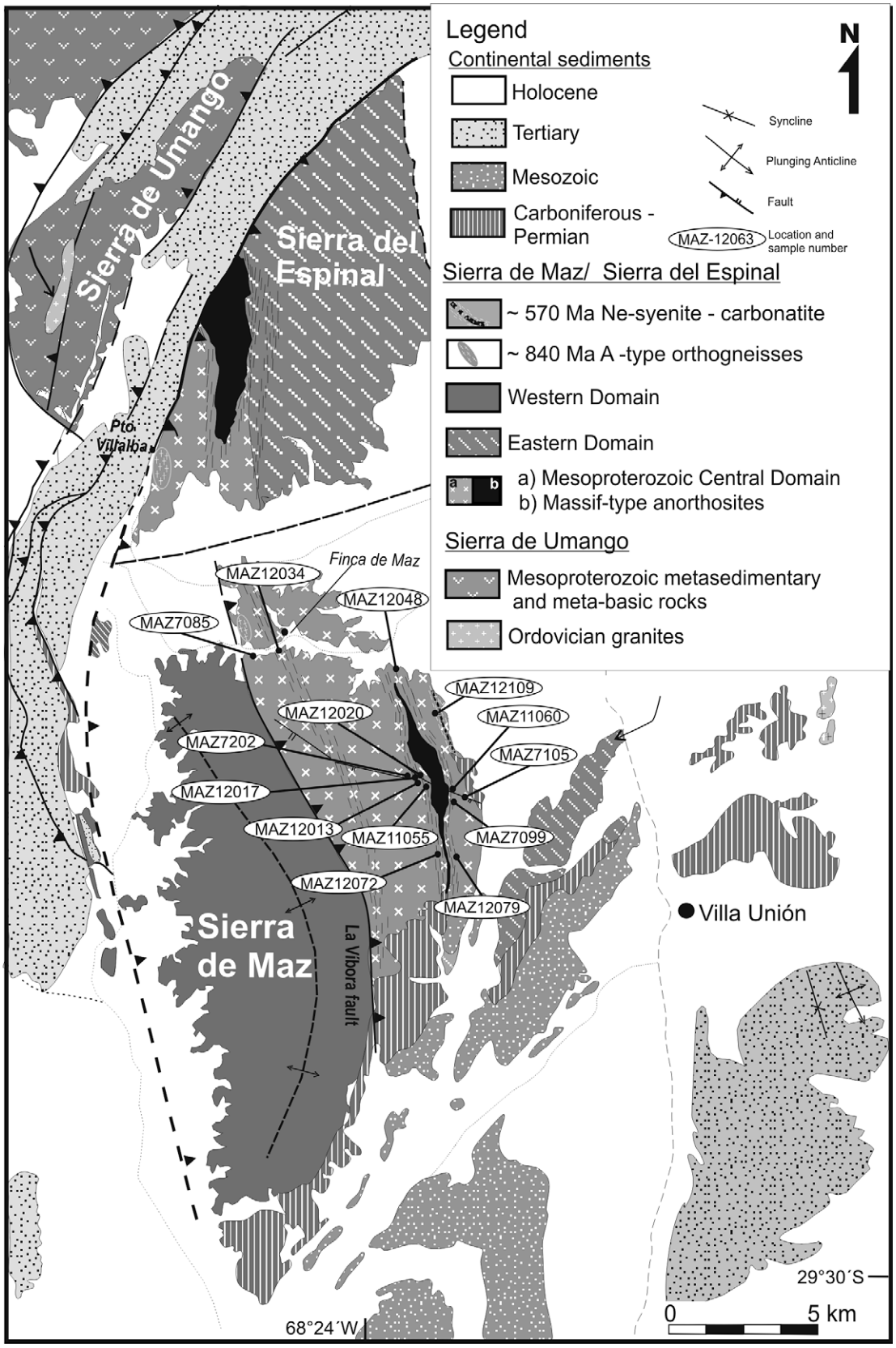

Fig. 2. Geological map of the Sierras Maz, Espinal and Umango, modified after Casquet et al. (2006, 2008), with the location of samples considered in this work (Tables 1 and 4).

Based on geochemical data, Vujovich and Kay (1998) interpreted the overall Grenville-age rocks of Pie de Palo as formed in an oceanic arc/back-arc complex similar to those in the western Pacific region. A U–Pb age of 1204 ± 5 Ma obtained in a gabbroic

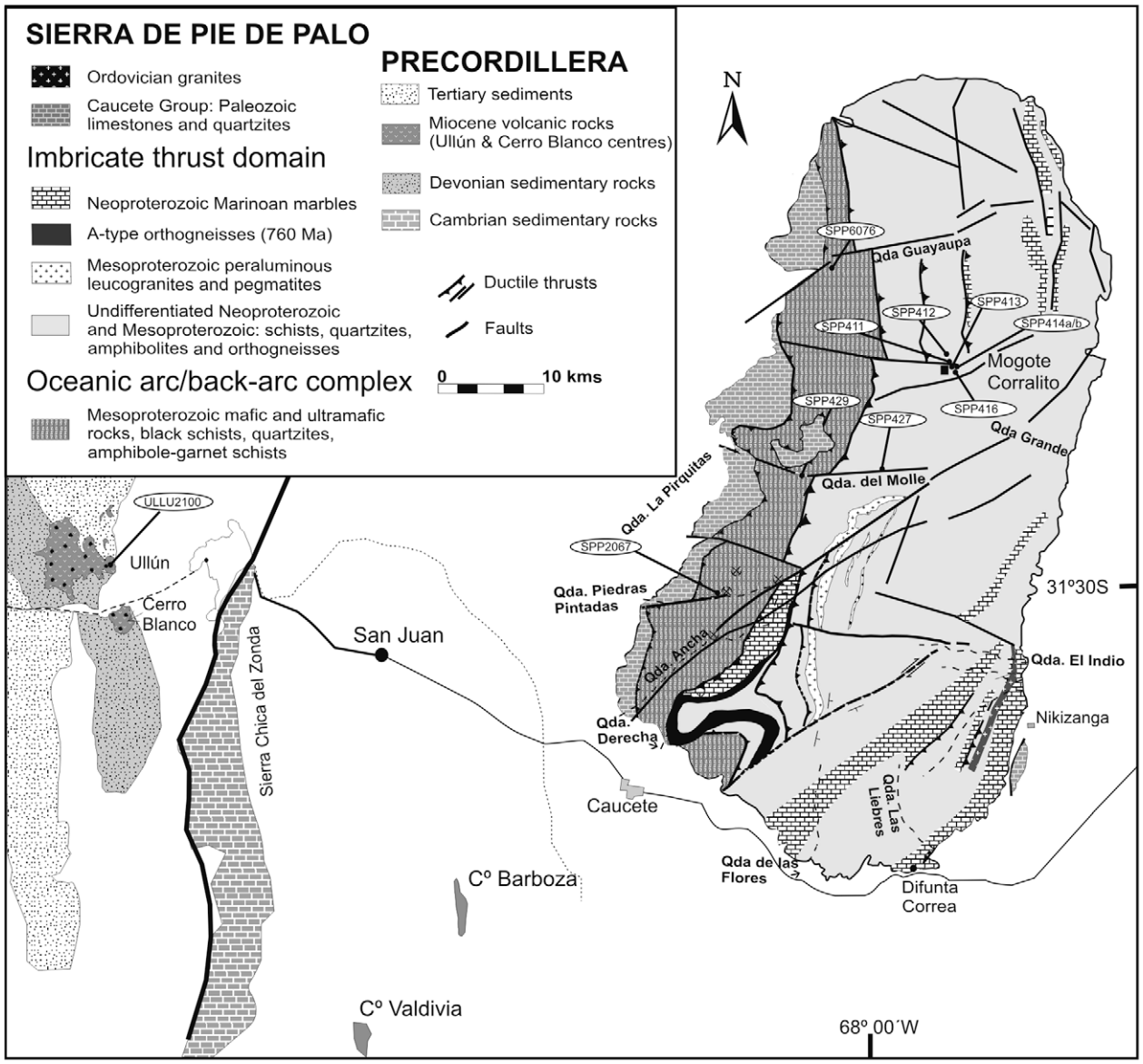

Fig. 3. Geological map of Sierra de Pie de Palo and adjacent Precordillera outcrops, modified after Vujovich and Kay (1998) and Baldo et al. (2006), with the location of samples considered in this work (Tables 3 and 4).

pegmatite of the lower unit constrains the timing of the assumed arc rifting and back-arc spreading stage (Vujovich et al., 2004). U–Pb ages of 1169 ± 8 and 1174 ± 43 Ma obtained from tonalitic–granodioritic sills and dykes that intrude both Mesoproterozoic domains were interpreted as representing either arc activity during and after back-arc spreading or a tectonically-unrelated arc (Vujovich et al., 2004).

2.3. The basement of the Precordillera: the Ullún xenoliths

The Cambrian and Early Ordovician sedimentary sequence of the Precordillera, located adjacent to the west of Sierra de Pie de Palo (Fig. 1), has no exposed underlying basement. Only indirect evidence of the age and composition of this basement comes from xenoliths included in Miocene dacitic to andesitic rocks that penetrated the Cambro-Ordovician strata. The best studied localities are the Ullún and Cerro Blanco volcanic centres described by Leveratto (1968) and Abruzzi et al. (1993), subsequently studied in more detail by Kay et al. (1996).

Metamorphic xenoliths, ranging in size from <3 cm up to 25 cm across, were considered by Abruzzi et al. (1993) and Kay et al. (1996) to have been mostly derived from mafic (SiO_2 = 48–54%) and felsic (SiO_2 = 69–71%) igneous protoliths. Three distinct xenolith suites were recognized:

(i) mafic pyroxene granulite and pyroxene–garnet granulite gneiss interpreted as derived from basaltic to basaltic–andesitic magmas formed in an oceanic back-arc or juvenile continental crustal back-arc setting.
(ii) deformed mafic amphibolitic schists interpreted as representing unfractionated mantle-derived arc magmas. An U–Pb zircon age for one sample from this suite yielded an upper intercept age of 1102 ± 6 Ma, which was considered a crystallization age. Two zircon fractions from the same sample, but with lower U and Pb concentrations, defined a ~1083 Ma $^{207}Pb/^{206}Pb$ age, interpreted as a metamorphic event.
(iii) biotite-bearing acid gneisses of dacitic composition interpreted as crustal melts. Zircon data from two samples of this

group are highly discordant: three fractions from one sample yield an upper intercept age of 1096 ± 50 Ma, while if the all six fractions from the samples are regressed together, the resulting upper intercept age is 1118 ± 54 Ma.

3. Geochemistry and Nd isotope data: tectonomagmatic affinities

3.1. Sierra de Maz

The database for Sierra de Maz consists of 26 new whole-rock chemical analyses and 12 Nd isotope determinations on selected samples of the main meta-igneous units of the Central Domain (see Tables 1 and 2 (data repository), and Fig. 2 for sample location). Amphibolites and orthogneisses of the Central Domain exhibit a silica range from 45% to 74% SiO_2 and can be subdivided in two main groups (Fig. 4). A first group of subalkaline samples (calcic to calc-alkaline fields, Fig. 4a and b), is composed of medium-K amphibolites (46–48% SiO_2), separated by a silica gap of 62–74% SiO_2 from mostly medium-K orthogneisses (Fig. 4c). This subalkaline group, as well as metasedimentary schists and gneisses, are the country rock of the anorthosite massif in the northeastern side of Sierra de Maz (Fig. 2).

A second group includes meta-anorthosites, meta-jotunites and an alkali-calcic series defined by high-K orthogneisses that plot in the monzonite and quartz monzonite fields of the plutonic TAS diagram (Fig. 4a and b). High-K amphibolites with shoshonite composition are tentatively linked to this group (Fig. 4c). Note that the massif-type meta-anorthosites of Sierra de Maz plot in the monzodiorite and monzogabbro fields (Fig. 4a). The trace element geochemistry and Nd isotope signature of both groups are described in more detail below (Figs. 5, 6 and 10).

3.1.1. Subalkaline series: Andean type, cordilleran granites and subduction-related basic rocks

The first group of subalkaline orthogneisses consists of metamorphosed diorites, tonalites, granodiorites and monzoganites, with SiO_2 62–74%, $Na_2O + K_2O$ 5.2–6.7%, FeOt + MgO 3–7%, REE patterns with $[La/Yb]_N = 10–45$ and a weak positive Eu anomaly ($Eu/Eu^* = 1.1–1.4$) (Table 1, Fig. 5a). The overall subalkaline geochemistry of these meta-granitic rocks is coupled with Ga/Al ($1000^*Ga/Al = 2.0–2.5$), FeOt/MgO (2–8), Zr/Nb (>17) and Ba/La (15–50) ratios that are characteristic of metaluminous magmas emplaced in convergent margins rather than intraplate settings (Pearce et al., 1984; Whalen et al., 1987; Eby 1990). Normalized to Ocean Ridge Granites (ORG) the subalkaline orthogneisses are enriched in K, Rb and Ba and depleted in Ta, Nb, Hf, Zr, Y, and Yb, which is also typical of arc-related magmas (Fig. 5b), in particular the cordilleran tonalitic to granitic suites (e.g., Hervé et al., 2007). The εNdt values range from +4.1 for the tonalite/diorite to −0.8 in the granodiorite and −7.2 in the granite (Fig. 6, Table 1). This indicates a significant amount of mature continental crust contamination of the acidic units, whereas the tonalite/diorite preserves the typical mantle signature of cordilleran tonalites.

The medium-K subalkaline amphibolites show some arc geochemical affinities, such as LILE- and Th enrichment and compatible element depletion when normalized against N-MORB, but they do not show other characteristics such as LREE enrichment and Nb depletion (Fig. 5c). εNdt varies from +3 to −1.5, with the typical range of Zr content for subalkaline rocks (30–60 ppm, Fig. 6). As in the case of the subalkaline orthogneisses, this variation in εNdt correlates with an increase of silica content, from 45.8% to 48.5% (Fig. 4, Table 1), again suggesting crustal contamination of the original basic magmas. These subalkaline meta-basic rocks, and the meta-granitic suite, have the typical igneous lithology formed in convergent margins such as the southern Andes, where basalt and basaltic-andesite stratovolcanoes and cordilleran batholiths largely constitute the edge of the continent (Hervé et al., 2007).

3.1.2. Alkali-calcic orthogneisses and massif-type anorthosites: an AMCG complex

The high-K alkali-calcic orthogneisses and amphibolites of the Central Domain show all the geochemical characteristic of a magmatic series that is transitional to the alkaline field. The orthogneisses are meta-monzonite and meta-quartz monzonites with SiO_2 57.1–68.4%, $Na_2O + K_2O$ 6.8–8.6%, FeOt + MgO 3.8–9.2%, REE patterns with $[La/Yb]_N = 3–15$ and a positive Eu anomaly ($Eu/Eu^* = 1.1–1.7$) (Table 1, Fig. 5a). This mild alkaline signature is also observed in the relatively high contents of incompatible elements, both LILE and HFSE (Fig. 5b), and the high ratios of Ga/Al ($1000^*Ga/Al = 2.5–3.5$) and FeOt/MgO (7–25) are diagnostic of A-type granites and, generally, of acidic within-plate magmatism (Pearce et al., 1984; Leat et al., 1986; Whalen et al., 1987; Eby, 1990). The Zr content has been considered useful for the recognition of alkaline signatures in rhyolitic rocks, and low-Zr (<300 ppm) rocks are termed "subalkaline", while high-Zr (>350 ppm) are classed as "peralkaline" (Leat et al., 1986). The Zr content of the high-K orthogneisses is very high (450–1150 ppm), and they also have εNdt values of +0.3 and −4.5 (Fig. 6), the latter indicating participation of the crust in the granitic source. Hypersthene-bearing monzonite and granitic rocks with intraplate signatures are often associated with massif-type anorthosites, producing the so-called AMCG complex (Anorthosites–Mangerites–Charnockites–Granites) (Emslie, 1978), which are common in the Grenville province of Canada (Corrigan and Hanmer, 1997; Rivers, 1997) and in the Appalachian Grenvillian basement. The original anorthosites, monzonites and quartz monzonites of Sierra de Maz underwent a Lower Paleozoic medium to high-grade event that transformed the original fabric and mineralogy during the docking of the Western Sierras Pampeanas against Gondwana (Casquet et al., 2008a). It is considered here that the high-K alkali-calcic orthogneisses and adjacent anorthositic massif of Sierra de Maz (Fig. 2) formed an intraplate AMCG complex, emplaced during a single broad magmatic episode (see geochronological section).

3.1.3. The Maz massif anorthosite

The anorthositic massif of Sierra de Maz (Fig. 2) was first described by Casquet et al. (2004). Although this body has been also affected by Lower Paleozoic medium to high-grade metamorphism and deformation, it is one of the best preserved Grenville-age magmatic units of the Western Sierras Pampeanas. Original relationships between the different anorthositic facies and the related mafic jotunites are still recognized, so that mathematical modelling of igneous geochemical trends can be used to constrain the fractional crystallization history. A refinement of the data and model presented by Casquet et al. (2004) is based on 12 new chemical analyses reported in Table 2 (data repository).

The main facies of the anorthosites is dominated by intermediate plagioclase showing sparse small pockets of mafic minerals. Occasionally, the proportion of mafic minerals increases, forming a jotunite groundmass with plagioclase phenocrysts or synplutonic dykes within the main facies. The bulk leucocratic anorthosites have high Al_2O_3 (23.5–27.5%) and Sr (720–930 ppm), and low to moderate K_2O (0.4–1.5%). They display moderately LREE-enriched chondrite-normalized patterns ($La/Yb_N = 32–5$) and positive Eu anomalies ($Eu/Eu^* = 13.5–2.5$) (Fig. 7a). The SiO_2-poor jotunites (SiO_2 38.9–48.1%) are enriched in FeO, TiO_2, MgO, P_2O_5, Zr, Hf, and Ta, and depleted in Al_2O_3, Na_2O, and Sr; their REE patterns are enriched in total REE with a slight negative to positive Eu anomaly ($Eu/Eu^* = 0.85–1.1$) (Figs. 4 and 7a). The Nd isotope compositions of the anorthosites and jotunites are variable: εNdt = +3.4

Table 1
Geochemical and isotope data of orthogneisses and amphibolites from Sierra de Maz.

	Subalkaline Series								Alkali-calcic Series					
	Amphibolites			Orthogneisses					Amphibolites			Orthogneisses		
Sample (wt%)*	12,079	7202	7105	7099	11,060	12,109	12,013	12,048	12,034	7085	12,017	12,020	11,055	12,072
SiO_2	45.87	48.38	48.54	62.14	62.26	66.27	72.04	73.66	45.06	47.18	54.11	57.11	57.67	68.45
TiO_2	1.15	0.44	1.15	0.64	0.59	0.74	0.50	0.26	1.80	1.86	2.38	1.29	1.03	0.47
Al_2O_3	17.13	16.54	12.86	17.80	17.67	14.60	13.56	14.11	14.03	15.33	12.72	15.93	16.56	15.17
Fe_2O_3t	13.36	11.53	16.22	4.64	4.25	5.68	3.87	2.58	14.90	12.93	16.01	10.43	8.54	3.62
MnO	0.17	0.18	0.21	0.07	0.06	0.09	0.06	0.04	0.21	0.20	0.27	0.18	0.17	0.05
MgO	6.57	8.19	6.26	2.27	1.99	2.02	0.43	0.65	10.79	7.14	1.70	1.01	0.81	0.44
CaO	11.22	9.93	10.82	5.57	5.49	4.09	2.46	2.61	8.49	8.17	6.05	5.42	4.96	2.12
Na_2O	1.71	1.98	1.99	4.89	4.78	3.31	2.66	3.05	1.14	2.84	2.04	3.99	3.76	2.86
K_2O	0.95	0.96	0.89	1.24	1.35	2.04	4.12	2.16	1.29	2.66	2.28	2.88	3.77	5.73
P_2O_5	0.12	0.10	0.13	0.18	0.16	0.24	0.15	0.06	0.34	0.38	1.24	0.52	0.32	0.19
LOI	1.20	1.35	0.44	0.58	2.70	0.75	0.49	0.87	1.69	1.35	0.34	0.92	2.42	1.01
Total (ppm)*	99.45	99.58	99.51	100.02	101.3	99.83	100.34	100.05	99.74	100.04	99.14	99.68	100.01	100.11
Cs	0.1	0.2	n.d	0.4	0.3	0.3	0.1	0.4	1.6	0.7	0.5	0.2	0	0.4
Rb	12	27	4	20	33	59	60	34	33	59	57	31	33	132
Sr	428	264	117	824	888	586	284	494	57	247	304	468	584	403
Ba	265	173	108	640	596	1273	1416	1636	114	431	797	2735	5592	2995
La	11.6	4.8	3.9	11.5	11.6	43.2	90.4	43	5.59	11.2	81.2	54.1	38.3	35.8
Ce	21.8	11.7	9.1	27.6	24.7	85	182	80.4	16.4	31	193	131	83.6	70.7
Pr	3.25	1.68	1.45	2.93	3.05	9.12	19.90	7.86	2.41	3.63	24.60	17.10	10.70	8.29
Nd	13.2	8.4	7.7	13.1	12.7	33.1	72.6	25.4	12.7	17.6	105	73.8	47.9	32.7
Sm	3.07	2.57	2.61	2.59	2.51	5.41	10.9	3.57	3.7	4.8	21	15	9.97	6.19
Eu	1.00	1.04	0.94	0.91	0.99	1.93	3.29	1.3	1.71	1.79	4.94	5.9	7.44	3.3
Gd	2.75	3.08	3.55	2.09	2.14	4.01	7.86	2.21	4.24	5.29	18.5	13.5	10.3	5.32
Tb	0.49	0.58	0.75	0.3	0.31	0.59	1.13	0.26	0.79	0	3.08	2.21	1.54	0.74
Dy	2.95	3.39	4.84	1.53	1.59	3.1	5.74	1.28	4.94	5.17	17.50	12.30	8.16	3.84
Ho	0.57	0.71	1.06	0.28	0.29	0.59	1.00	0.24	0.94	1.03	3.22	2.26	1.6	0.73
Er	1.60	1.97	3.21	0.81	0.85	1.66	2.72	0.71	2.64	2.86	9.19	6.3	4.55	1.92
Tm	0.23	0.30	0.51	0.11	0.12	0.22	0.37	0.1	0.38	0.4	1.34	0.87	0.65	0.26
Yb	1.42	1.82	3.21	0.77	0.78	1.38	2.48	0.65	2.39	2.63	8.33	5.42	4.17	1.56
Lu	0.22	0.28	0.52	0.11	0.11	0.21	0.39	0.1	0.35	0.40	1.27	0.84	0.62	0.22
U	0.34	0.15	0.04	0.09	0.04	0.19	0.49	0.44	0.27	0.6	0.5	0.59	0.5	0.4
Th	1.15	0.53	n.d	0.2	0.05	5.59	4.59	7.48	0.43	1.03	1.94	1.28	1.12	0.97
Y	15.8	19.6	31.8	8.0	9.0	15.2	25.2	5.8	26.1	28.2	91.5	64.1	41.5	19.0
Nb	2.6	4.6	6.2	6.0	3.0	5.4	15.0	2.9	5.7	7.6	64.9	106	48.2	7.7
Zr	43	56	62	124	89	273	435	149	96	140	863	1101	1150	450
Hf	1.5	1.6	1.9	3.1	2.3	6.8	11.2	4.2	2.7	3.2	18.1	25.9	24.8	10.4
Ta	0.14	0.68	0.08	0.12	0.13	0.21	0.45	0.09	3.71	0.34	3.85	6.9	4.5	0.47
Sc	38	54	52	8	8	12	10	4	26	28	28	24	19	5
Ga	21	17	16	19	21	17	18	15	18	16	24	27	22	23
Ni	40	137	80	n	n	30	20	20	240	74	20	130	n	20
Co	40	56	56	13	33	13	4	3	65	44	18	11	16	5
Cr	50	318	81	32	n	60	20	90	690	214	20	20	n	80
Pb	5	n	n.d	8	249	12	15	30	5	7	9	12	7	23
Nd isotope data**														
Sm (ppm)		2.57	2.61	2.59			10.9	3.57	3.7	4.8		15.0		6.19
Nd (ppm)		8.41	7.67	13.1			72.60	25.4	12.7	17.6		73.8		32.7
$^{147}Sm/^{144}Nd$		0.1847	0.2057	0.1195			0.0907	0.0849	0.1761	0.1649		0.1229		0.1144
$^{143}Nd/^{144}Nd$		0.512532	0.512634	0.512212			0.511726	0.511351	0.512601	0.512513		0.512123		0.511819
εNdt		−0.1	−1.5	4.1			−0.8	−7.2	2.2	2.0		0.3		−4.5

All Sample Nos. have the prefix MAZ
Minor elements determined by ICP–MS spectrometry.
*Analyses carried out by ACTMajor elements determined by ICP spectrometry.
**Analytical methods as in Galindo et al. (2004). $^{143}/^{144}Nd$ measured on sector 54 mass spectrometer. Analytical errors (2a) are 0.2% and 0.0006% for the $^{147}Sm/^{144}Nd$ and $^{143}/^{144}Nd$, respectively.

to −1.2 indicating a probable mantle source with moderate contamination by old continental crust (Casquet et al., 2004). A refined model of trace element fractional crystallization in which a sample of the main facies (MAZ12052, Table 2) and the jotunites are late stage residual liquids, is presented in Fig. 7b. The modelled daughter melts after 80%, 90%, and 95% crystallization predict an increase in REEt and Zr, a decrease in the initial positive Eu anomaly, which becomes slightly negative at 95% crystallization, and a decrease in the positive Sr anomaly, which becomes negative for the residual melts at 90–95% crystallization (Fig. 7b). Patterns displayed by the SiO_2-poor jotunites (SiO_2 39–42%, Fig. 7a) are very similar to the modelled residual melts, in the production of which Zr behaves as an incompatible element.

3.1.4. Alkali-calcic amphibolites

Alkali-calcic amphibolites with SiO_2 45.1–54.1%, K_2O 1.3–2.7 and Na_2O-2.0 ⩽ K_2O (Table 1 and Fig. 1c) show affinities with the shoshonitic series (Ewart, 1982; Le Maitre, 1989). Samples with SiO_2 45–47% have REE patterns with $[La/Yb]_N$ = 2–2.5 and weak positive Eu anomalies (Eu/Eu^* = 1.1–1.3), while a sample with 54% SiO_2 shows an enriched pattern with $[La/Yb]_N$ = 7 and a negative Eu anomaly (Eu/Eu^* = 0.75) (Table 1, Fig. 5a). Normalized against

Table 2
Geochemical and isotope data of the anorthositic massif of Sierra de Maz.

Sample (wt%)*	Anorthosites								Jotunites			
	12,050	12,027	12,053	12,073	12,024	12,023	12,052	12,068	12,025	12,049	12,028	12,026
SiO_2	51.17	52.54	53.12	53.52	53.82	54.11	54.61	55.05	38.91	39.10	39.30	48.11
TiO_2	1.53	0.88	0.12	0.61	0.10	0.28	0.10	0.28	3.61	3.69	3.59	2.02
Al_2O_3	23.72	23.81	26.77	25.46	26.36	26.15	27.56	25.39	13.81	11.82	11.70	17.40
Fe_2O_3t	6.93	5.85	1.03	2.83	1.07	2.09	0.77	1.46	22.80	25.30	25.04	17.12
MnO	0.13	0.09	0.02	0.04	0.01	0.03	0.01	0.02	0.28	0.41	0.41	0.30
MgO	1.08	1.4	0.21	0.52	0.1	0.29	0.06	0.22	4.07	3.89	3.91	2.58
CaO	9.27	8.97	9.71	9.36	9.09	9.57	10.34	8.68	11.07	9.90	9.37	8.44
Na_2O	4.3	4.41	4.82	4.67	5.3	5.27	5.06	5.25	1.13	2.81	2.40	2.58
K_2O	0.65	0.54	1.13	0.85	0.88	0.89	0.63	1.04	0.59	0.56	0.54	0.46
P2O5	0.27	0.12	0.04	0.08	0.08	0.09	0.04	0.07	2.33	2.60	2.11	1.13
LOI	0.77	0.87	2.09	1.65	1.75	1.59	0.91	1.58	0.09	0.26	0.57	0.11
Total (ppm)*	99.82	99.48	99.06	99.59	98.56	100.36	100.09	99.04	98.69	100.34	98.94	100.25
Cs	0.3	0.2	0.5	1.2	2.6	1.5	0.2	2.3	0.1	0.1	0.1	0.1
Rb	7	5	18	13	15	18	5	17	2326			
Sr	727	745	927	763	838	812	857	801	123	582	553	437
Ba	287	247	543	299	323	270	264	436	55	509	424	150
La	9.93	6.29	4.32	6.27	5.24	6.52	4.25	6.51	81.7	62.9	54.2	27.5
Ce	22.6	12.8	9	12.4	9.9	12.9	8.0	12.5	222.0	167.0	144.0	68.6
Pr	2.93	1.47	1.06	1.40	1.06	1.44	0.86	1.39	32.60	24.20	20.80	9.18
Nd	12.60	6.03	4.04	5.34	4.03	5.71	3.11	5.15	154.0	111.0	99.2	41.1
Sm	2.49	1.19	0.82	1.02	0.70	1.06	0.48	0.88	35.20	25.20	22.30	8.96
Eu	2.37	1.84	1.06	2.25	1.68	1.74	1.95	1.91	9.84	8.02	7.70	2.46
Gd	2.42	1.16	0.71	0.93	0.51	0.90	0.40	0.76	31.90	25.00	20.80	8.46
Tb	0.38	0.20	0.11	0.15	0.08	0.15	0.06	0.12	5.53	3.87	3.31	1.49
Dy	2.19	1.22	0.66	0.86	0.39	0.82	0.29	0.65	30.30	20.90	18.30	8.31
Ho	0.43	0.25	0.13	0.17	0.07	0.15	0.05	0.12	5.41	3.78	3.28	1.59
Er	1.23	0.73	0.36	0.48	0.17	0.42	0.14	0.34	14.70	9.82	8.51	4.50
Tm	0.18	0.12	0.05	0.07	0.00	0.06	0.00	0.05	1.97	1.22	1.10	0.65
Yb	1.17	0.82	0.33	0.48	0.11	0.39	0.12	0.28	11.00	7.12	6.29	4.15
Lu	0.18	0.13	0.05	0.08	0.02	0.06	0.02	0.04	1.57	1.02	0.90	0.66
U	0.09	0.03	0.07	0.10	0.01	0.08	0.08	0.03	0.11	0.29	0.30	0.18
Th	0.14	0.27	0.35	0.25	0.05	0.10	0.18	0.13	0.24	1.04	0.63	0.37
Y	11.60	7.10	3.50	4.60	1.80	4.20	1.40	3.50	147.0	92.1	87.4	44.7
Nb	16.4	8.5	1.4	4.5	1.2	3.5	0.8	2.4	58.3	19.0	19.5	24.4
Zr	51	30	40	54	4	6	6	21	232	157	150	42
Hf	1.1	0.7	0.9	1.3	0.1	0.3	0.2	0.5	8.2	5.3	5.2	1.2
Ta	1.20	0.59	0.14	0.34	0.02	0.15	0.05	0.15	3.18	1.55	1.39	1.54
Sc	8	8	1	4	1	2	1	2	51	55	58	23
Ga	20	20	18	21	22	21	21	25	27	26	26	22
Ni	20	20	20	20	20	20	20	20	40	20	30	30
Co	11	12	1	5	1	3	1	2	27	23	21	26
Cr	70	100	20	30	20	20	40	30	20	20	20	20
Pb	5	5	5	5	5	5	5	5	5	5	5	5
Nd isotope data**												
Sm (ppm	2.49						0.48			25.2		
Nd (ppm)	12.6						3.1			111.0		
$^{147}Sm/^{144}Nd$	0.1195						0.0933			0.0997		
$^{143}/^{144}Nd$	0.512219						0.511939			0.512332		
εNdt	2.4						0.5			2.2		

All Sample Nos. have the prefix MAZ.
Minor elements determined by ICP–MS spectrometry.
*Analyses carried out by ACTL major elements determined by ICP spectrometry.
**Analytical methods as in Galindo et al. (2004). $^{143}/^{144}Nd$ measured on Sector 54 mass spectrometer. Analytical errors (2σ) are 0.2% and 0.0006% for the $^{147}Sm/^{144}Nd$ and $^{143}/^{144}Nd$, respectively.
Analytical errors (2σ) are 0.2% and 0.0006% for the $^{147}Sm/^{144}Nd$ and $^{143}/^{144}Nd$, respectively.

N-MORB these rocks are enriched in LILE and LREE (Fig. 5c) and have high abundances of HFSE elements, particularly the most acidic sample (MAZ12017, SiO_2 = 54%, Nb = 65 ppm, and Ta = 3.9 ppm, Table 1).

3.2. Sierra de Pie de Palo

The geochemistry and Nd isotope composition of the orthogneisses and mafic units from Sierra de Pie de Palo (Fig. 3) are based on of 12 new analyses (Table 3, Data Repositary) and previous results reported by Vujovich and Kay (1998) and Vujovich et al. (2004).

3.2.1. The oceanic arc/back-arc complex

In the lower mafic-ultramafic unit of Sierra de Pie de Palo (Fig. 3), amphibolites with N-MORB, back-arc like, geochemical signatures are common (pattern field, Fig. 9a and b) (Vujovich and Kay, 1998). However, both in the lower unit and in the overlaying imbricate thrust domain, there are also abundant subalkaline amphibolites and metagabbros that do not display the same geochemical characteristics (calcic field, Fig. 8). These latter rocks, including the SHRIMP-analysed gabbro sample SPP2067, show SiO_2 = 44.5–53.3%, K_2O = 0.2–1.1%, Al_2O_3 11.4–17.1% and REE patterns with $[La/Yb]_N$ = 0.6–2.7 and Eu/Eu^* = 0.75–1.06) (Table 3, Fig. 9a). Normalized against N-MORB they are enriched in LILE,

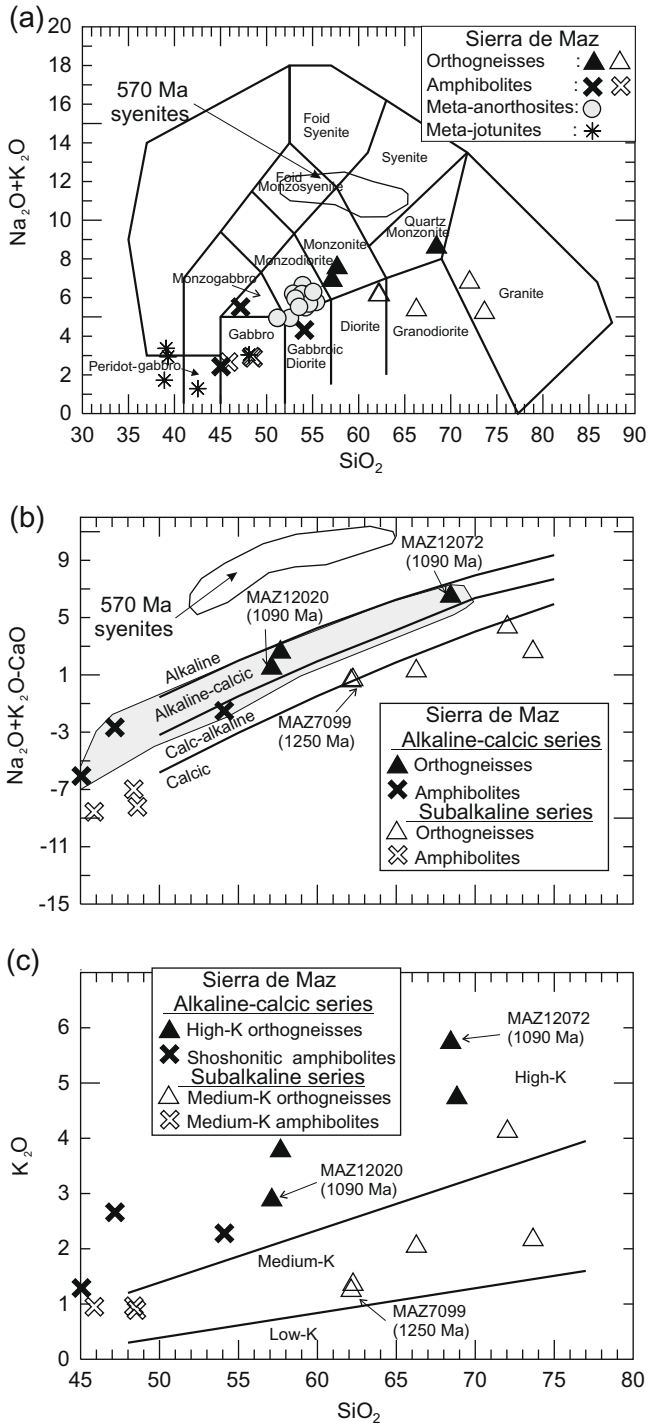

Fig. 4. Harker plots for the meta-igneous rocks of Sierra de Maz. Dividing lines and fields are from: (a) Middlemost (1997), (b) Frost et al. (2001), and (c) Le Maitre (1989). Identified samples in (b) and (c) are those with U–Pb SHRIMP ages determined in this study.

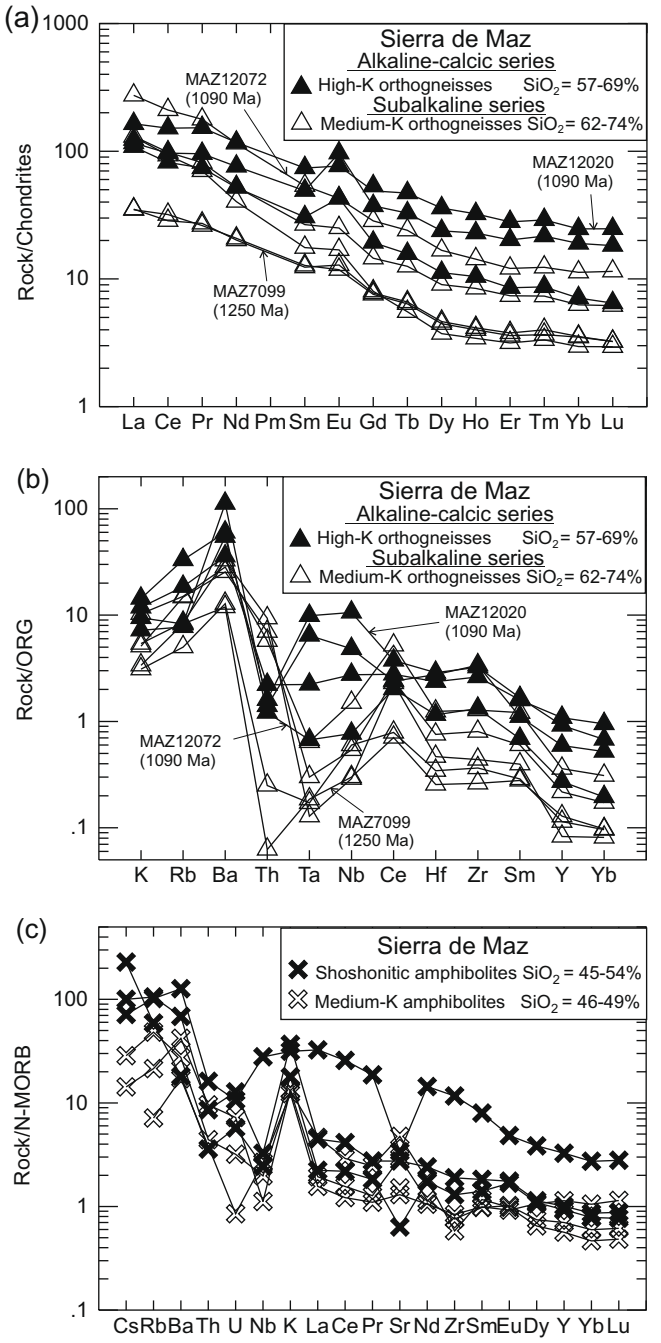

Fig. 5. Trace-element abundances in meta-igneous rocks of Sierra de Maz normalized to (a) chondrites (Nakamura, 1974), (b) ocean ridge granite (ORG, Pearce et al., 1984), and (c) N-MORB (Sun and McDonough, 1989). Identified samples in (a) and (b) are those with U–Pb SHRIMP ages determined in this study.

Th and LREE elements, which is taken as evidence that they formed in a supra-subduction zone environment, although they do not show the Nb depletion of many arc basalts (Fig. 9b). The pattern of the 1204 ± 5 Ma VL38 metagabbro dated by Vujovich et al. (2004) is also shown for comparison. A depleted mantle source is inferred for the calcic arc-related amphibolites and metagabbros (εNdt = +4.5 to +8, Fig. 6). This suggests that the lower mafic–ultramafic unit is probably built on complex stacking of arc and back-arc rocks (Vujovich and Kay, 1998).

3.2.2. Arc-related calc-alkaline orthogneisses

Subordinate and sparse outcrops of a calc-alkaline orthogneiss series can be distinguished in Sierra de Pie de Palo. The dated sample SPP6076 is a calc-alkaline orthogneiss (Fig. 8) that shows a moderately steep REE pattern ($[La/Yb]_N = 12.5$) with well-developed middle REE depletion and a weak negative Eu anomaly, suggesting amphibole and feldspar fractionation (Fig. 10a). It is enriched in LREE and Ba, and shows negative Nb and Sr anomalies when normalized against N-MORB (Fig. 10b). The 1108 ± 13 Ma calc-alkaline orthogneisses from Sierra de Umango studied by Varela et al. (2003) show similar but even steeper REE patterns (Fig. 10b), suggesting equilibration with a garnet-bearing residue.

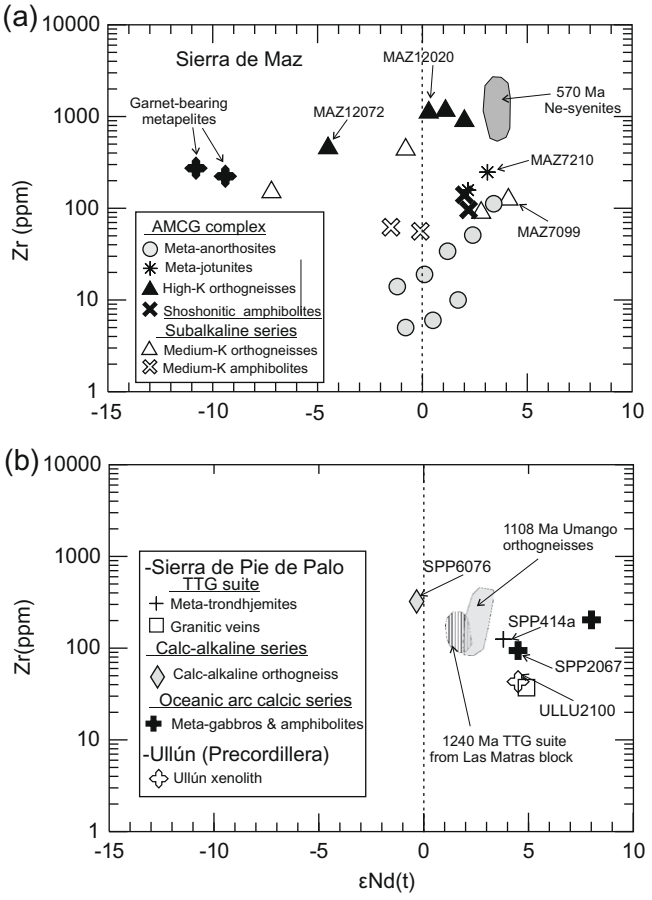

Fig. 6. Variation of εNdt vs log Zr (ppm) for (a) the meta-igneous rocks of Sierra de Maz and (b) meta-igneous rocks of Sierra de Pie de Palo, an Ullún xenolith (Precordillera). Garnet-bearing metapelites and the field for 570 Ma Ne-syenites of Sierra de Maz are from Casquet et al. (2008a,b), respectively. Identified samples in (a) and (b) are those with U–Pb SHRIMP ages determined in this study. The age and Zr content of the jotunite MAZ7210 is from Casquet et al. (2004). The field for the TTG rocks of Las Matras block is from Sato et al. (2000), while the field of the Umango orthogneisses is from Varela et al. (2003).

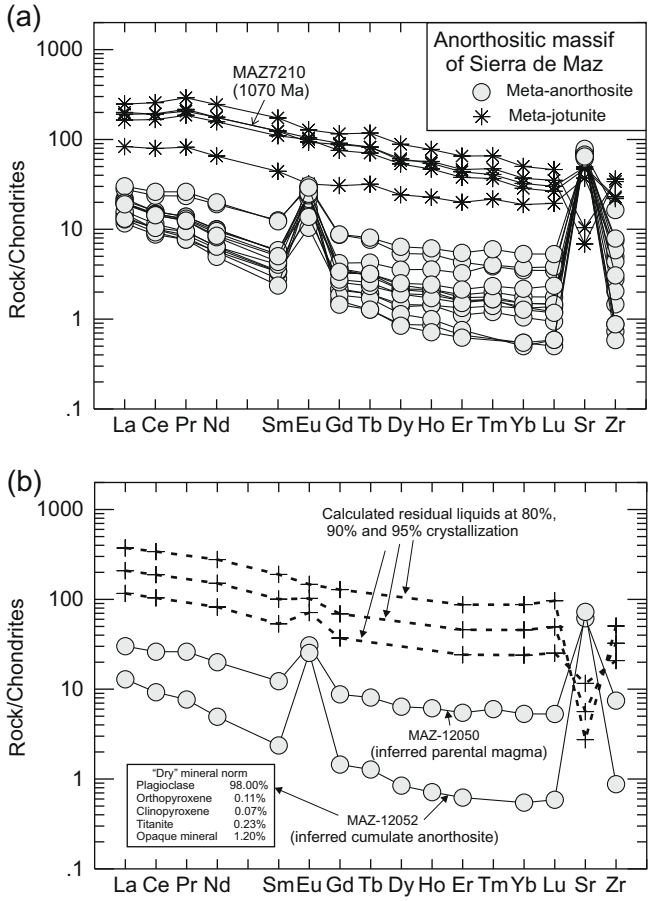

Fig. 7. (a) Chondrite-normalized REE, Sr and Zr patterns of meta-anorthosites and jotunites from Sierra de Maz (data from Table 2 and Casquet et al., 2004), (b) modelled residual liquids formed by Rayleigh fractional crystallization of a parental anorthosite (main facies, sample MAZ12050, Table 2) and an extracted cumulate assemblage represented by the leucocratic anorthosite MAZ12052. See text for further details. The jotunite MAZ7210 is from Casquet et al. (2004).

Subduction under more mature crust is the preferred tectonic environment for this magmatism, which shows the least juvenile Nd isotope signature in this sierra (εNdt = −0.2, Fig. 6b).

3.2.3. The Mogote-Corralito TTG suite

At the top of Sierra de Pie de Palo, within the imbricate thrust domain, a distinct sequence of metaluminous meta-trondhjemites and meta-tonalites forms the dominant lithology (Quebrada Mogote-Corralito, Fig. 3), with SiO_2 73.6–77.1%, Na_2O, 4.9–5.1%, FeOt + MgO 2.5–3.3%, REE patterns with $[La/Yb]_N$ = 2.3–3.0 and a negative Eu anomaly ($Eu/Eu^* = 0.56–0.72$) (Table 3, Fig. 10c). Associated leucocratic granitic veins that plot on the same Rb–Sr isochron (Pankhurst and Rapela, 1998), show a negative slope of the REE patterns (Fig. 10c), suggesting fractionation of a LREE-rich accessory mineral such as allanite during the late crystallization stages. Allanite is an accessory mineral in the host trondhjemites. A mantle signature is indicated by the low $^{87}Sr/^{86}Sr$ initial ratio (0.7045, Pankhurst and Rapela, 1998), which is confirmed by a juvenile εNdt of +3.8 for the meta-trondhjemite sample dated by U–Pb SHRIMP in this study (SPP414a, Fig. 6). Generation of this TTG suite in an arc environment is consistent with the low abundances of HFSE such as Nb and Ta, low Ga/Al ratio ($1000^*Ga/Al$ = 0.7–2.2) and low Sr/Y (3.7–4.0) (Table 3), while the low $[La/Yb]_N$ ratios suggest a source outside the garnet stability field. Note that the 1244 ± 42 Ma metaluminous tonalites and trondhjemites from Las Matras block (Fig. 1, Sato et al., 2000, 2004) show similar but slightly steeper REE patterns $[La/Yb]_N$ = 3.7–5.5 (Sato et al., 2000) (Fig. 10c).

3.3. Precordillera basement: the Ullún xenoliths

The chemical analysis of a SHRIMP-dated foliated mafic xenolith enclosed in a Miocene dacite intruded in the Precordillera (sample ULLU2100, Fig. 3) is shown in Table 3 (data repository) and Figs. 6b, 8c and 9c. Relative to the compositions of the xenolith groups recognized in the same outcrops by Kay et al. (1996), the major and trace element abundances of sample ULLU2100 are very similar to the least siliceous samples of the mafic amphibolite group (SiO_2 = 47.7–50.9%, Figs. 8c and 9c), while the εNdt (+4.5) is slightly less primitive than those of the most mafic amphibolites (+3.2 to +3.5, Table 4 of Kay et al., 1996). Altogether these characteristics point to relatively unfractionated mantle-derived arc magmatic rocks for the protoliths of the amphibolites, as was first inferred by Abruzzi et al. (1993).

It is worth pointing out that a more siliceous mafic amphibolite xenolith sample described by Kay et al. (1996) (UZ93B, SiO_2 = 53.4%, εNd_t = +2.1, 1102 ± 6 Ma) (Fig. 8c), shows a distinct, steeper, REE pattern (Fig. 9c) that resembles that of the roughly coeval calc-alkalic orthogneiss of Sierra de Pie de Palo (SPP6076, SiO_2 = 68.2%, εNd_t = −0.2, 1110 ± 10 Ma) (Fig. 10a and b), which is

Table 3
Geochemical and isotope data of Sierra de Pie de Palo and Ullum xenolith (Precordillera).

	Pie de Palo											Ullum Xenolith
	Oceanic arc rocks				Mogote-Corralito meta-trondhjemites				Granitic veins		Calc-alkaline orthogneiss	
	Amphibolites		Metagabbro									
Sample	429	423	427	2067	412	414a	411	416	413	414b	6076	2100
(wt%)	*	*	*	**	*	*	*	*	*	*	**	**
SiO_2	44.5	47.58	47.98	53.25	73.64	74.11	76.36	77.15	73.61	74.92	68.24	50.12
TiO_2	3.17	1.07	2.11	0.81	0.19	0.21	0.17	0.17	0.01	0.02	0.52	0.70
Al_2O_3	11.35	16.16	12.98	17.07	12.48	12.32	12.2	11.92	14.04	14.16	15.31	14.08
Fe_2O_3t	20.81	11.79	16.01	7.79	2.87	3.52	2.78	2.73	0.35	0.72	4.36	10.05
MnO	0.33	0.18	0.26	0.14	0.1	0.11	0.07	0.08	0.03	0.07	0.09	0.22
MgO	7.61	8.86	6.07	6.69	0.13	0.16	0.19	0.1	0.01	0.01	0.95	8.18
CaO	9.5	10.18	9.46	9.08	1.64	1.71	1.45	1.29	0.95	0.98	2.48	9.21
Na_2O	1.71	2.88	2.48	3.27	5.08	4.97	4.89	5.11	5.2	4.85	3.48	3.06
K_2O	0.24	0.73	0.79	1.1	1.49	1.51	1.81	1.43	4	4.34	4.37	1.24
P_2O5	0.21	0.11	0.21	0.11	0.04	0.05	0.04	0.03	0.01	0.01	0.21	0.57
LOI	1.31	1.08	0.56	0.91	0.28	0.22	0.24	0.24	0.28	0.34	0.82	2.20
Total (ppm)*	100.74	100.62	98.91	100.22	97.94	98.89	100.2	100.25	98.49	100.42	100.83	99.63
Cs	0.2	1.6	1.4	0.5	1.0	1.1	1.0	1.3	36.5	0.5	0.40	0.4
Rb	1	11	39	28	45	41	62	28	97	88	97	25
Sr	95	223	95	289	131	122	117	100	91	105	210	755
Ba	90	95	162	242	330	370	500	450	420	326	1222	212
La	8.90	3.60	7.00	9.24	10.70	11.80	10.50	13.00	1.80	1.60	50.60	7.73
Ce	26.0	11.0	25.0	22.6	25.0	28.0	24.0	32.0	6.0	6.0	100.0	16.60
Pr	n.d	n.d	n.d	3.37	n.d	n.d	n.d	n.d	n.d	n.d	11.90	2.94
Nd	18.00	8.00	18.00	14.20	14.00	16.00	13.00	16.00	4.00	3.00	39.50	12.60
Sm	5.02	2.40	6.15	3.59	3.53	3.70	2.96	4.06	1.08	0.91	7.20	3.33
Eu	1.65	0.94	1.85	1.34	0.78	0.86	0.65	0.78	0.39	0.37	1.60	0.95
Gd	n.d	n.d	n.d	4.04	n.d	n.d	n.d	n.d	n.d	n.d	6.00	3.26
Tb	1.10	0.60	1.70	0.67	0.80	0.70	0.50	0.70	0.40	0.30	0.89	0.51
Dy	n.d	n.d	n.d	4.12	n.d	n.d	n.d	n.d	n.d	n.d	4.93	2.96
Ho	n.d	n.d	n.d	0.85	n.d	n.d	n.d	n.d	n.d	n.d	0.96	0.60
Er	n.d	n.d	n.d	2.48	n.d	n.d	n.d	n.d	n.d	n.d	2.81	1.83
Tm	n.d	n.d	n.d	0.35	n.d	n.d	n.d	n.d	n.d	n.d	0.42	0.27
Yb	4.07	2.49	7.95	2.17	2.73	3.32	2.49	2.95	3.29	2.70	2.66	1.69
Lu	0.60	0.37	1.18	0.31	0.41	0.50	0.36	0.46	0.51	0.42	0.38	0.24
U	0.40	0.10	0.10	0.83	0.90	0.80	0.50	0.40	0.50	1.60	2.38	0.99
Th	0.70	0.20	0.70	0.87	2.10	1.30	1.10	1.40	3.40	2.50	12.00	0.45
Y	43.00	25.00	72.00	23.20	33.00	34.00	29.00	28.00	28.0	28.0	28.9	18.9
Nb	6.0	8.0	10.0	5.5	4.0	2.0	2.0	2.0	2.0	2.0	10.3	5.7
Zr	203	78	173	94	128	125	135	149	37	83	314	43
Hf	4.1	1.6	4.4	2.4	3	3.3	2.8	3.5	0.9	2	7.3	1.7
Ta	0.30	0.30	0.30	0.32	0.30	0.30	0.60	0.30	0.30	0.30	0.58	0.66
Sc	46	37	48	27	12	12	8	10	3	1	8	36
Ga	16	10	9	16	15	15	5	14	18	19	18	14
Ni	82	139	50	0	50	50	50	50	50	50	0	100
Co	59	44	53	26	1	1	2	1	0.5	0.4	7	29
Cr	177	121	123	380	80	57	67	62	37	17	15	290
Pb	n.d	n.d	n.d	7	n.d	n.d	n.d	n.d	n.d	n.d	11	32
Nd isotope	***			***		***			***		****	***
Sm (ppm)	5.02			3.41		4.06			1.15		7.2	4.53
Nd (ppm)	18			13.69		19.08			2.97		39.5	18.03
^{147}Sm /144N	0.1686			0.1505		0.1459			0.2350		0.1376	0.1520
$^{143}/^{144}Ni$	0.512827			0.512502		0.512493			0.513146		0.512201	0.512550
εNdt	8			4.5		3.8			4.9		-0.2	4.5

Pie de Palo samples have the prefix SPP; the xenolith is ULLU2100.
Minor elements determined by INAA.
*** Analyses carried out by ACTLABS, Canada. * Major elements determined by XRF.
** Major elements determined by ICP spectrometry. Minor elements dtermined by ICP-MS spectrometry.
*** Analytical methods as in Pankhurst and Rapela (1995): Sm and Nd by MS isotope dilution at NIGL: (±1%, 1σ) $^{143}/^{144}Nd$ measured on MAT 262 (±0.005%, 1σ).
**** Analytical methods as in Galindo et al. (2004). $^{143}/^{144}Nd$ measured on Sector 54 mass spectrometer. Analytical errors (2a) are 0.2% and 0.0006% for the ^{147}Sm /^{144}Nd and $^{143}/^{144}Nd$, respectively.

however more siliceous and does not show the typical high Cr and Ni contents of the mafic amphibolite xenolith group.

4. U–Pb zircon geochronology

4.1. Samples and method

Sampling for SHRIMP U–Pb zircon dating was designed to provide information on crystallization ages of the main magmatic series recognized in the sierras of Maz and Pie de Palo (Figs. 8–10), and of a xenolith interpreted as derived from the basement of the Precordillera (Fig. 8c and 10c). Under CL imaging the sectioned zircon grains were seen to have metamorphic overgrowths, so an additional aim was to constrain the timing of metamorphism. Sample localities are shown in the maps (Figs. 2 and 3); precise coordinates and a short description of the mineralogy and fabric for each sample are provided in the following section. Mineral abbreviations follow Kretz (1983).

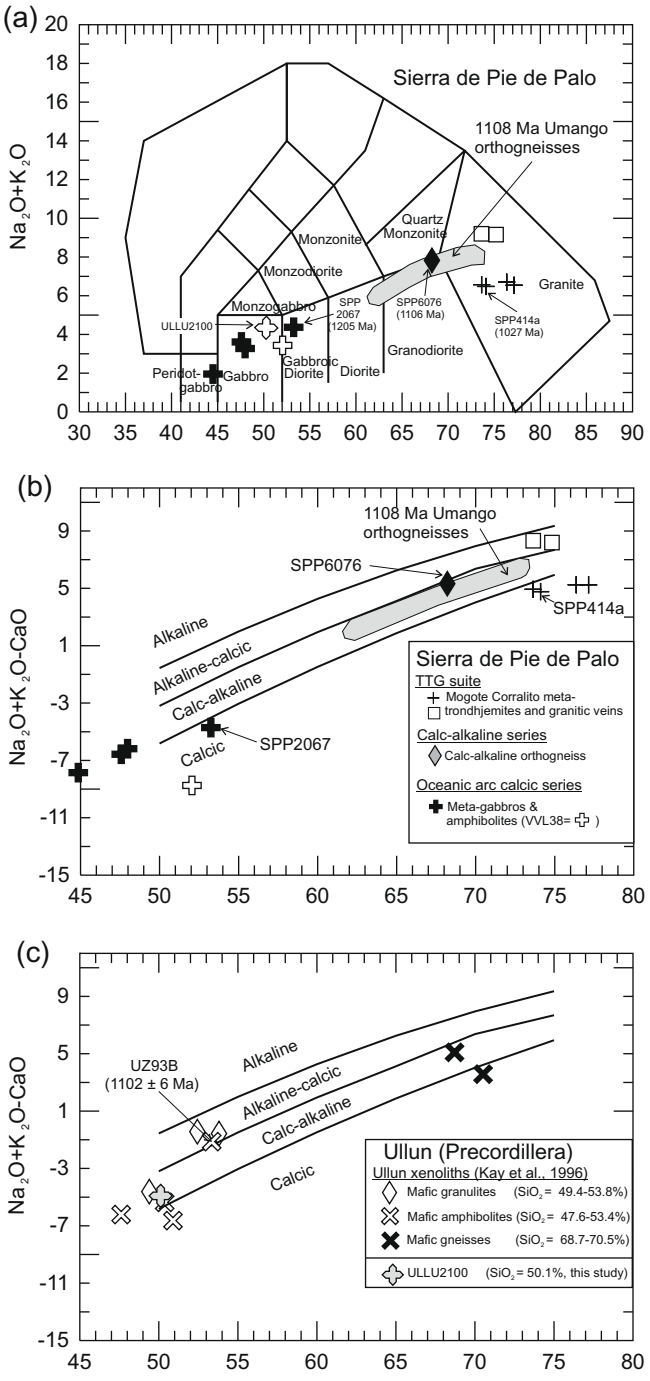

Fig. 8. Harker plots for the meta-igneous rocks of Sierra de Pie de Palo (a and b) and Ullún xenoliths in the Precordillera (c). Dividing lines and fields are from: (a) Middlemost (1997) and (b and c) Frost et al. (2001). Identified samples are those with U–Pb SHRIMP ages determined in this study, while metagabbro VV38 and shoshonite amphibolite PP10 from Sierra de Pie de Palo are from Vujovich et al. (2004) and Vujovich and Kay (1998), respectively. Ullún xenoliths from the Precordillera are from Kay et al. (1996). The field of Umango orthogneisses is from Varela et al. (2003).

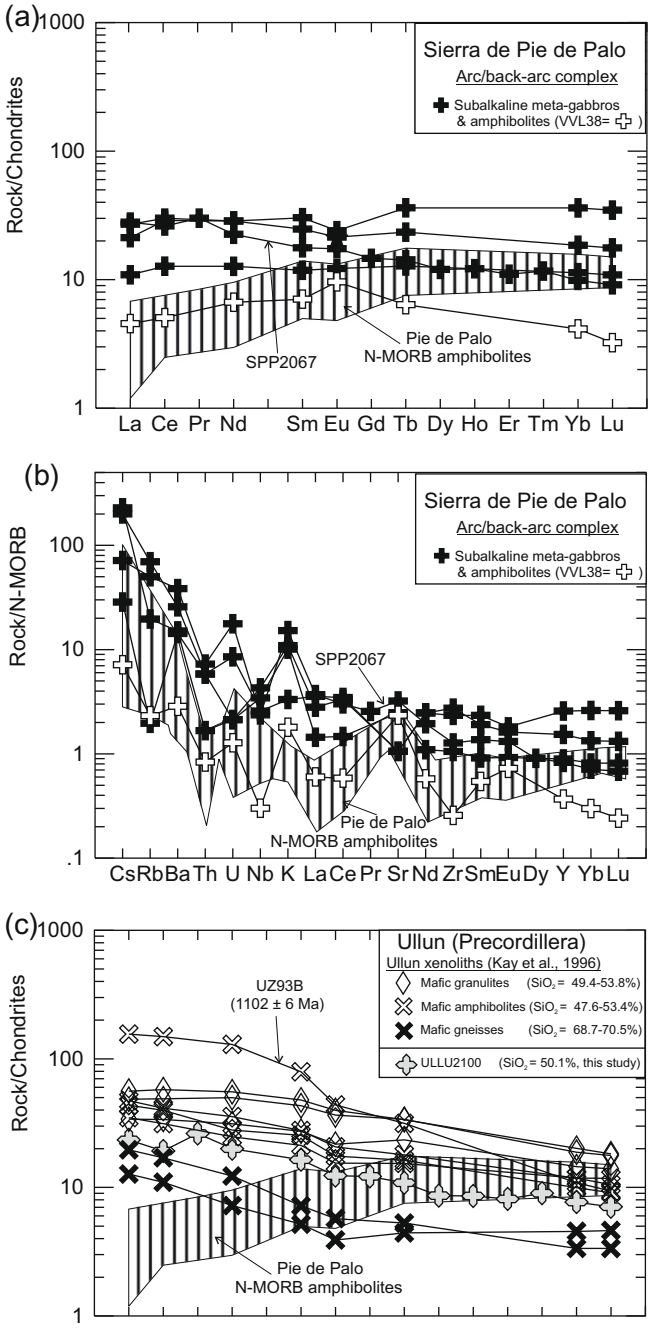

Fig. 9. (a) Trace element abundances in the arc/back-arc meta-igneous rocks of Sierra de Pie de normalized to chondrites (Nakamura, 1974), (b) Trace element abundances in the arc/back-arc meta-igneous rocks of Sierra de Pie de Palo normalized to N-MORB (Sun and McDonough, 1989). The fields of N-MORB amphibolites from Sierra de Pie de Palo in (a) and (b) are from Vujovich and Kay (1998), and (c) Trace elements abundances in the Ullún xenoliths of the Precordillera and U–Pb dated xenolith UZ93B are after Kay et al. (1996). The field of N-MORB amphibolites from Sierra de Pie de Palo is that of Vujovich and Kay (1998). Identified samples are those with U–Pb SHRIMP ages determined in this study, while metagabbro VV38 from Sierra de Pie de Palo is from Vujovich et al. (2004).

The separated zircons were mounted in epoxy together with reference zircons, sectioned and polished. U–Th–Pb analyses were made using SHRIMP II or SHRIMP RG at the Research School of Earth Sciences, The Australian National University, Canberra, following methods given in Williams (1998) and references therein. Cathodo-luminescence (CL) images were prepared for all zircon grains and were used to target specific areas for analysis. The data were processed using the SQUID Excel macro (Ludwig 2001). U–Pb data are given in Table 4 (data repository); details of the reference zircons used to calibrate the U/Pb ratios and the calibration uncertainties are also given in data repository tabulations. Uncertainties in Table 4 for individual analyses (ratios and ages) are at the one-sigma level.

Wetherill Concordia plots, probability density plots with stacked histograms, and weighted mean and Concordia age calculations were carried out using Isoplot/Ex (Ludwig, 2003); age

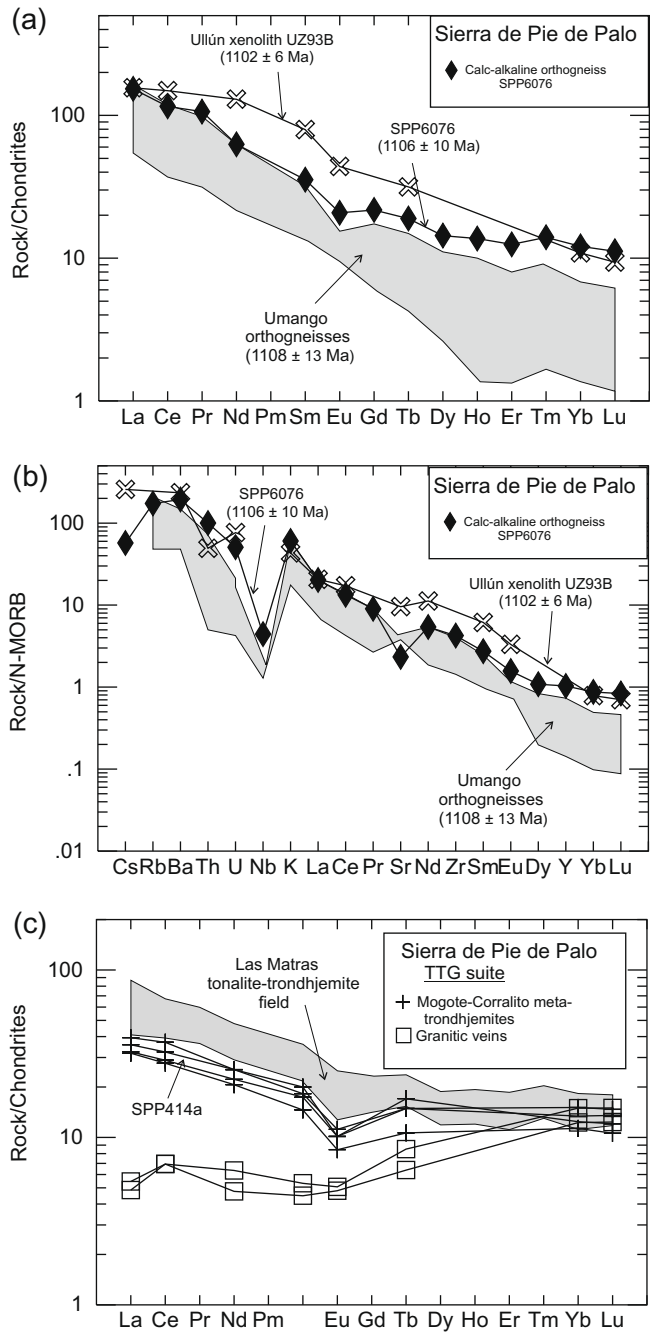

Fig. 10. (a) Trace element abundances in calc-alkaline meta-igneous rocks of Sierra de Pie de Palo normalized to chondrites (Nakamura, 1974) and (b) N-MORB (Sun and McDonough, 1989). The fields of Umango orthogneisses are from Varela et al. (2003) and the Ullún xenolith is from Kay et al. (1996). (c) Trace element abundances in meta-trondhjemites and related granitic veins from Sierra de Pie de Palo normalized to chondrites. The field for the 1244 ± 42 Ma tonalite–trondhjemites from Las Matras block (Fig. 1) is from Sato et al. (2000). Identified samples are those with U–Pb SHRIMP ages determined in this study.

uncertainties are reported as 95% confidence limits. In some cases, the "mixture modelling" algorithm of Sambridge and Compston (1994) was used (via Isoplot/Ex) to statistically separate age populations or groupings. Due to the difficulty in determining precise, common Pb corrected, radiogenic $^{207}Pb/^{206}Pb$ ratios for ca. 1 Ga zircons by SHRIMP, a range of techniques was employed to calculate individual best age estimates. The choice of technique was based on factors such as the U content of the zircon area analysed (which flows onto the amount of radiogenic ^{207}Pb), the ability to detect ^{204}Pb, the strength of the primary ion beam used for the analysis, and whether the area analysed is considered to have lost radiogenic Pb, etc. This is discussed below on a sample-by-sample basis.

4.2. Analytical results

MAZ7099, Sierra de Maz (29°16′ 06.4″, 68°21′ 09.1″). This sample is a subalkaline, medium-K, metadioritic orthogneiss (Fig. 4); its main mineralogy is Pl–Qtz–Hbl–Cpx–Bt–Ttn–Ep, with accessory Op, Ap, and Zrn. The original granular igneous fabric is still preserved, but an amphibolite-facies coronitic texture with Cpx, Anf, Pl, and myrmekitic Ep is also well developed. Zircons are large (~200 μm across) and sub-round to somewhat elongated, often with faceted forms. A summary of the initial results was presented by Casquet et al. (2005) but a re-interpretation is presented here, taking into account a larger database.

The zircons from this sample show complex internal structure under CL (Fig. 11). In general the grains have an igneous component that shows weak oscillatory zoning (as core/centres), which in places is overgrown by a sector-zoned zircon component reflecting a high-grade metamorphic paragenesis. Some grains are dominated by the metamorphic zircon component. A few grains have thin bright luminescent rims that are significantly less than 10 microns in width and so difficult to analyse.

The analyses cluster close to or within uncertainty of Concordia (Wetherill plot) and have $^{207}Pb/^{206}Pb$ ages ranging from ca. 980 to ca. 1290 Ma. The U content is variable, ranging up to 300 ppm, but many areas analysed have less than 44 ppm U. The Th content is covariant and, whilst the CL images indicate a metamorphic paragenesis, the Th/U ratios are in the range of normal igneous zircon (ca. 0.4–0.8). This suggests that the high-grade metamorphic zircon growth has occurred without significant Th depletion, a feature that has been documented previously (see Goodge et al., 2001). The low U contents make it difficult to determine precise $^{207}Pb/^{206}Pb$ ratios and ages. Given the general concordance of the analyses, our preferred treatment of this low U data-set is based on the radiogenic $^{206}Pb/^{238}U$ ages, as shown in the probability density plot (inset Fig. 11). There is a poorly defined older grouping of dates, with one peak at about 1260 Ma and a subordinate one at about 1330 Ma. These generally correspond to the core analyses and are taken reflecting the time of igneous crystallization of the orthogneiss protolith. Two younger groupings are better defined as discrete events, one at ca. 1175 Ma and a younger at ca.1095 Ma. These younger ages are interpreted as representing metamorphic events, the older of which was probably at rather high-grade on the basis of the metamorphic zircon morphology.

MAZ12020, Sierra de Maz (29°15′ 37.3″, 68°22′ 19.6″). This is an alkali-calcic, high-K meta-monzonitic (meta-mangerite) orthogneiss (Fig. 4b and c). Its main mineralogy is Pl–Hbl–Grt–Qtz (<20%) – Bt, with accessory Ttn, Czo, Ilm, Zrn, and Ap. The metamorphic assemblage Grt + Bt + Pl + Hbl indicates garnet amphibolite facies conditions.

The zircons from this sample are notably elongate, subhedral grains, up to 400 μm in length, most with sub-round terminations. Many grains have colourless inclusions of apatite. The CL images show either simple oscillatory zoning or areas with broad zones, sometimes rimmed by oscillatory zonation. These features are interpreted as reflecting a single igneous zircon crystallisation event. The 19 grains analysed, including cores and rims to three structured grains, yield concordant to near-concordant data (Fig. 12a, Table 4). Eighteen of the 21 areas analysed form a single concordant grouping to within analytical uncertainty, giving a Concordia age of 1092 ± 6 Ma (MSWD = 0.23), which constrains the time of igneous zircon crystallisation. There is no evidence within these zircon grains for metamorphic growth. However the subhedral grain shape and sub-round nature of terminations suggests

Table 4
U–Pb SHRIMP Zircon Analytical Data for Western Sierras Pampeanas (data repository) SHRIMP Data.

Grain. spot	U (ppm)	Th (ppm)	Th/U	$^{206}Pb^{*}$ (ppm)	$^{204}Pb/^{206}Pb$	f_{206} %	Total Ratios				Radiogenic Ratios						ρ	Age (Ma)				
							$^{238}U/^{206}Pb$	±	$^{207}Pb/^{206}Pb$	±	$^{206}Pb/^{238}U$	±	$^{207}Pb/^{235}U$	±	$^{207}Pb/^{206}Pb$	±		$^{206}Pb/^{238}U$	±	$^{207}Pb/^{206}Pb$	±	% Disc
(a) Summary of SHRIMP U–Pb zircon results for sample MAZ7099																						
2003 SHRIMP II																						
1.1	133	51	0.38	24.5	0.000117	0.19	4.663	0.054	0.0848	0.0006	0.2141	0.0025	2.455	0.040	0.0832	0.0009	0.715	1250	13	1273	22	2
2.1	300	176	0.59	50.9	–	<0.01	5.060	0.054	0.0796	0.0004	0.1976	0.0021	2.170	0.026	0.0796	0.0004	0.900	1163	11	1188	10	2
3.1	24	12	0.52	4.5	0.000407	0.68	4.456	0.076	0.0850	0.0015	0.2241	0.0038	2.592	0.063	0.0839	0.0015	0.698	1304	22	1290	34	−1
4.1	27	15	0.56	4.9	0.000310	0.52	4.703	0.077	0.0826	0.0014	0.2128	0.0035	2.445	0.057	0.0833	0.0014	0.706	1244	20	1277	32	3
4.2	25	13	0.53	3.8	0.000610	1.05	5.688	0.097	0.0797	0.0015	0.1747	0.0030	1.792	0.050	0.0744	0.0016	0.608	1038	18	1052	45	1
5.1	132	153	1.16	24.7	0.000114	0.19	4.600	0.053	0.0843	0.0006	0.2170	0.0025	2.474	0.038	0.0827	0.0008	0.752	1266	13	1262	20	0
5.2	48	20	0.42	8.5	0.000158	0.26	4.799	0.067	0.0859	0.0011	0.2078	0.0029	2.398	0.059	0.0837	0.0017	0.575	1217	16	1286	39	5
6.1	42	22	0.51	7.0	0.000305	0.51	5.209	0.075	0.0844	0.0011	0.1910	0.0028	2.110	0.071	0.0801	0.0024	0.434	1127	15	1200	60	6
6.2	18	10	0.54	2.5	–	<0.01	6.033	0.114	0.0795	0.0018	0.1658	0.0031	1.828	0.054	0.0800	0.0018	0.643	989	17	1196	44	17
7.1	26	14	0.55	3.9	0.000133	0.22	5.612	0.093	0.0793	0.0015	0.1778	0.0030	1.898	0.073	0.0774	0.0027	0.437	1055	16	1133	69	7
7.2	22	11	0.53	3.7	0.000115	0.19	5.015	0.086	0.0830	0.0015	0.1990	0.0035	2.232	0.086	0.0813	0.0028	0.451	1170	19	1230	68	5
8.1	19	10	0.49	3.1	0.000079	0.13	5.401	0.099	0.0815	0.0018	0.1849	0.0034	2.049	0.095	0.0804	0.0034	0.403	1094	19	1206	83	9
8.2	309	35	0.11	48.4	0.000001	<0.01	5.479	0.059	0.0764	0.0004	0.1825	0.0020	1.921	0.024	0.0763	0.0005	0.875	1081	11	1104	12	2
9.1	17	8	0.50	2.7	0.000753	1.30	5.341	0.100	0.0785	0.0018	0.1858	0.0035	1.839	0.061	0.0718	0.0020	0.565	1098	21	981	56	−12
2008 SHRIMP RG																						
10.1	32	15	0.47	5.8	0.000473	0.80	4.785	0.087	0.0837	0.0014	0.2073	0.0038	2.200	0.082	0.0770	0.0025	0.488	1214	20	1120	65	−8
3.2	87	40	0.46	15.0	0.000054	0.09	4.998	0.066	0.0786	0.0009	0.1999	0.0026	2.146	0.041	0.0779	0.0011	0.693	1175	14	1143	27	−3
11.1	74	34	0.45	12.7	0.000291	0.49	5.043	0.070	0.0824	0.0009	0.1973	0.0028	2.131	0.056	0.0783	0.0017	0.534	1161	15	1155	44	0
11.2	115	91	0.80	19.9	0.000197	0.33	4.953	0.063	0.0808	0.0007	0.2012	0.0026	2.166	0.040	0.0780	0.0010	0.691	1182	14	1148	26	−3
12.1	264	130	0.49	45.0	0.000026	0.04	5.044	0.057	0.0809	0.0006	0.1982	0.0022	2.200	0.030	0.0805	0.0006	0.827	1165	12	1210	15	4
12.2	49	34	0.69	9.7	0.000515	0.86	4.369	0.068	0.0877	0.0012	0.2269	0.0035	2.517	0.072	0.0804	0.0019	0.541	1318	19	1208	48	−9
4.3	29	16	0.54	4.7	0.000601	1.02	5.349	0.101	0.0834	0.0017	0.1851	0.0037	1.909	0.140	0.0748	0.0053	0.269	1095	20	1064	142	−3
13.1	195	109	0.56	31.0	0.000076	0.13	5.394	0.064	0.0783	0.0006	0.1852	0.0022	1.972	0.030	0.0772	0.0007	0.780	1095	12	1127	19	3
13.2	31	15	0.49	6.0	0.000628	1.05	4.443	0.078	0.0877	0.0014	0.2252	0.0043	2.732	0.119	0.0880	0.0028	0.773	1309	22	1383	60	5
14.1	33	17	0.52	5.5	0.001466	2.60	5.098	0.098	0.0809	0.0016	0.1947	0.0041	2.016	0.123	0.0751	0.0036	0.741	1147	22	1070	95	−7
9.2	37	17	0.46	7.0	0.000962	1.64	4.530	0.081	0.0859	0.0015	0.2196	0.0042	2.470	0.119	0.0816	0.0029	0.750	1280	22	1235	71	−4
15.1	22	11	0.51	3.6	0.000905	1.58	5.366	0.121	0.0788	0.0020	0.1850	0.0046	1.857	0.138	0.0728	0.0043	0.722	1094	25	1009	120	−8
16.1	74	37	0.50	13.6	0.000345	0.58	4.652	0.068	0.0855	0.0010	0.2137	0.0031	2.376	0.057	0.0806	0.0015	0.610	1249	17	1213	37	−3
17.1	58	46	0.79	11.0	0.000237	0.39	4.561	0.071	0.0848	0.0011	0.2184	0.0034	2.453	0.067	0.0815	0.0018	0.579	1273	18	1233	44	−3
18.1	97	90	0.92	18.7	0.000179	0.30	4.479	0.061	0.0840	0.0009	0.2226	0.0031	2.499	0.050	0.0814	0.0012	0.683	1296	16	1232	29	−5
Error in FC1 reference zircon calibration was 0.43% & 0.55% for the two analytical sessions.																						
(b) Summary of SHRIMP U–Pb zircon results for sample MAZ 12072.																						
1.1	84	52	0.62	13.1	0.000148	0.25	5.520	0.067	0.0772	0.0007	0.1807	0.0022	1.870	0.035	0.0751	0.0011	0.655	1071	12	1070	28	0
2.1	298	161	0.54	46.6	0.000013	0.02	5.505	0.066	0.0762	0.0004	0.1816	0.0022	1.903	0.025	0.0760	0.0004	0.908	1076	12	1095	11	2
3.1	527	187	0.36	80.2	–	<0.01	5.650	0.059	0.0753	0.0003	0.1770	0.0019	1.841	0.021	0.0754	0.0003	0.933	1051	10	1080	8	3
4.1	116	105	0.91	18.3	0.000032	0.05	5.460	0.063	0.0767	0.0006	0.1830	0.0021	1.924	0.028	0.0762	0.0007	0.797	1084	12	1102	18	2
5.1	111	104	0.93	17.1	0.000209	0.35	5.593	0.065	0.0776	0.0007	0.1782	0.0021	1.834	0.038	0.0746	0.0013	0.569	1057	11	1059	34	0
6.1	56	53	0.94	8.8	–	<0.01	5.484	0.072	0.0763	0.0009	0.1825	0.0024	1.942	0.036	0.0772	0.0010	0.704	1081	13	1125	27	4
7.1	77	74	0.96	12.0	–	<0.01	5.474	0.068	0.0783	0.0008	0.1828	0.0023	1.991	0.033	0.0790	0.0009	0.739	1082	12	1172	22	8
8.1	73	103	1.41	11.1	0.000154	0.26	5.663	0.071	0.0767	0.0008	0.1761	0.0022	1.810	0.039	0.0745	0.0013	0.591	1046	12	1056	35	1
9.1	108	59	0.55	16.8	–	<0.01	5.523	0.065	0.0764	0.0007	0.1811	0.0021	1.911	0.028	0.0765	0.0007	0.800	1073	12	1109	18	3
14.1	95	81	0.85	14.8	–	<0.01	5.538	0.078	0.0767	0.0007	0.1806	0.0025	1.918	0.033	0.0770	0.0007	0.827	1071	14	1121	19	5
12.2	264	128	0.49	43.8	0.000859	1.45	5.173	0.066	0.0886	0.0005	0.1905	0.0025	2.007	0.058	0.0764	0.0020	0.452	1124	13	1106	51	−2
15.1	87	87	1.00	13.4	0.000147	0.25	5.597	0.073	0.0776	0.0008	0.1782	0.0023	1.854	0.037	0.0755	0.0011	0.659	1057	13	1081	30	2
16.1	114	137	1.21	17.2	0.000029	0.05	5.666	0.170	0.0762	0.0007	0.1764	0.0053	1.844	0.059	0.0758	0.0008	0.940	1047	29	1090	22	4
17.1	199	97	0.49	30.6	0.000015	0.02	5.583	0.063	0.0741	0.0005	0.1791	0.0020	1.824	0.025	0.0739	0.0005	0.839	1062	11	1038	15	−2
17.2	90	61	0.68	14.5	0.000052	0.09	5.311	0.082	0.0753	0.0008	0.1881	0.0029	1.934	0.040	0.0746	0.0010	0.744	1111	16	1057	28	−5
18.1	69	54	0.79	11.2	0.000068	0.11	5.287	0.070	0.0752	0.0009	0.1889	0.0025	1.933	0.036	0.0742	0.0010	0.710	1116	14	1047	27	−7
19.1	83	59	0.71	12.7	–	<0.01	5.595	0.072	0.0763	0.0008	0.1788	0.0023	1.897	0.033	0.0769	0.0009	0.740	1061	13	1119	23	5
20.1	126	74	0.59	20.6	0.000015	0.03	5.240	0.063	0.0759	0.0007	0.1908	0.0023	1.991	0.030	0.0757	0.0007	0.794	1126	12	1087	18	−4

20.2	288	118	0.41	45.9	0.000039	0.07	5.390	0.059	0.0759	0.0004	0.1854	0.0020	1.927	0.025	0.0754	0.0005	0.846	1096	11	1079	14	−2
21.1	68	80	1.17	11.3	0.000035	0.06	5.195	0.090	0.0770	0.0009	0.1924	0.0033	2.030	0.044	0.0765	0.0010	0.800	1134	18	1109	26	−2
21.2	80	55	0.69	12.5	0.000078	0.13	5.457	0.086	0.0756	0.0008	0.1830	0.0029	1.879	0.039	0.0745	0.0010	0.767	1083	16	1054	26	−3
22.1	60	52	0.86	9.4	0.000010	0.02	5.450	0.074	0.0744	0.0010	0.1835	0.0025	1.879	0.035	0.0743	0.0010	0.725	1086	14	1049	26	−3
23.1	138	177	1.29	21.0	0.000115	0.20	5.625	0.066	0.0756	0.0006	0.1774	0.0021	1.809	0.030	0.0739	0.0008	0.719	1053	11	1040	23	−1

Error in Temora reference zircon calibration was 0.36% and 0.61% for the analytical sessions.
NB due to a multiplier malfunction analyses of grains 10–13 were not considered meaningful

(c) Summary of SHRIMP U–Pb zircon results for sample MAZ 12020.

1.1	63	42	0.67	10.0	–	<0.01	5.401	0.093	0.0781	0.0009	0.1853	0.0032	2.006	0.042	0.0785	0.0009	0.826	1096	17	1161	23	6
2.1	77	65	0.84	12.3	–	<0.01	5.369	0.066	0.0769	0.0008	0.1863	0.0023	1.975	0.032	0.0769	0.0008	0.756	1101	12	1119	21	2
2.2	124	156	1.25	19.5	0.000032	0.05	5.489	0.063	0.0770	0.0007	0.1821	0.0021	1.923	0.028	0.0766	0.0007	0.779	1078	11	1110	19	3
3.1	72	43	0.60	11.6	0.000035	0.06	5.331	0.066	0.0779	0.0010	0.1875	0.0023	2.000	0.038	0.0774	0.0011	0.655	1108	13	1130	28	2
3.2	127	154	1.22	19.4	0.000031	0.05	5.631	0.064	0.0763	0.0006	0.1775	0.0020	1.856	0.028	0.0758	0.0007	0.763	1053	11	1090	19	3
4.1	141	45	0.32	22.9	–	<0.01	5.286	0.060	0.0752	0.0006	0.1892	0.0021	1.963	0.027	0.0752	0.0006	0.822	1117	12	1075	16	−4
5.1	77	45	0.58	12.3	–	<0.01	5.364	0.077	0.0757	0.0008	0.1866	0.0027	1.964	0.036	0.0763	0.0009	0.785	1103	15	1104	23	0
6.1	94	55	0.59	15.2	0.000016	0.03	5.318	0.065	0.0764	0.0007	0.1880	0.0023	1.973	0.031	0.0761	0.0007	0.789	1110	12	1098	19	−1
7.1	102	80	0.79	16.1	–	<0.01	5.424	0.064	0.0763	0.0007	0.1846	0.0022	1.970	0.031	0.0774	0.0008	0.739	1092	12	1131	21	3
8.1	98	29	0.30	14.8	–	<0.01	5.691	0.069	0.0764	0.0007	0.1758	0.0021	1.857	0.028	0.0766	0.0007	0.791	1044	12	1111	19	6
9.1	106	54	0.51	17.0	0.000071	0.12	5.360	0.062	0.0764	0.0006	0.1863	0.0022	1.938	0.030	0.0754	0.0008	0.757	1102	12	1080	20	−2
10.1	90	61	0.68	14.3	0.000017	0.03	5.430	0.065	0.0755	0.0007	0.1841	0.0022	1.910	0.030	0.0752	0.0007	0.773	1089	12	1075	20	−1
11.1	159	53	0.33	25.3	0.000050	0.08	5.403	0.067	0.0765	0.0005	0.1849	0.0023	1.932	0.029	0.0758	0.0006	0.836	1094	12	1089	16	0
12.1	119	57	0.48	18.8	–	<0.01	5.443	0.063	0.0758	0.0006	0.1838	0.0021	1.935	0.028	0.0763	0.0007	0.794	1088	12	1104	18	1
13.1	63	41	0.65	10.0	0.000332	0.56	5.365	0.080	0.0799	0.0009	0.1853	0.0028	1.920	0.050	0.0752	0.0016	0.576	1096	15	1073	43	−2
14.1	40	31	0.76	6.3	0.000116	0.20	5.469	0.076	0.0749	0.0012	0.1831	0.0029	1.917	0.099	0.0759	0.0031	0.766	1084	16	1093	81	1
15.1	157	35	0.22	24.8	0.000013	0.02	5.447	0.061	0.0754	0.0006	0.1836	0.0021	1.903	0.027	0.0752	0.0007	0.787	1086	11	1074	18	−1
16.1	75	24	0.32	11.6	0.000047	0.08	5.548	0.068	0.0743	0.0008	0.1801	0.0022	1.827	0.034	0.0736	0.0010	0.666	1068	12	1030	28	−4
17.1	116	62	0.54	18.6	0.000026	0.04	5.375	0.062	0.0760	0.0006	0.1860	0.0022	1.939	0.029	0.0756	0.0007	0.771	1099	12	1085	19	−1
18.1	116	39	0.33	18.6	–	<0.01	5.370	0.062	0.0757	0.0006	0.1863	0.0022	1.961	0.030	0.0763	0.0007	0.767	1102	12	1103	19	0
19.1	82	56	0.68	12.8	0.000039	0.07	5.519	0.067	0.0752	0.0008	0.1811	0.0022	1.864	0.034	0.0747	0.0010	0.675	1073	12	1059	27	−1

Error in Temora reference zircon calibration was 0.36% for the analytical session.

(d) Summary of SHRIMP U–Pb zircon results for sample SPP2067.

1.1	539	124	0.23	93	0.000039	0.07	4.983	0.053	0.0814	0.0004	0.2006	0.0021	2.235	0.028	0.0808	0.0005	0.856	1178	11	1217	13	3
2.1	517	123	0.24	89	0.000024	0.04	4.976	0.052	0.0815	0.0004	0.2009	0.0021	2.247	0.027	0.0811	0.0005	0.866	1180	11	1224	12	4
3.1	324	71	0.22	55	0.000042	0.07	5.019	0.055	0.0808	0.0005	0.1991	0.0022	2.202	0.031	0.0802	0.0007	0.768	1170	12	1202	18	3
4.1	261	57	0.22	46	0.000108	0.18	4.851	0.054	0.0810	0.0005	0.2058	0.0023	2.254	0.035	0.0794	0.0008	0.726	1206	12	1183	21	−2
5.1	642	168	0.26	113	0.000004	0.01	4.864	0.051	0.0803	0.0003	0.2056	0.0022	2.275	0.026	0.0803	0.0003	0.926	1205	12	1203	8	0
6.1	306	69	0.23	54	0.000066	0.11	4.899	0.054	0.0812	0.0005	0.2039	0.0022	2.257	0.033	0.0803	0.0008	0.754	1196	12	1204	19	1
7.1	405	91	0.22	71	–	<0.01	4.869	0.053	0.0802	0.0005	0.2054	0.0022	2.275	0.029	0.0803	0.0006	0.841	1204	12	1205	14	0
8.1	159	26	0.17	28	0.000118	0.20	4.958	0.059	0.0812	0.0007	0.2013	0.0024	2.207	0.044	0.0795	0.0013	0.600	1182	13	1185	32	0
9.1	550	121	0.22	97	0.000082	0.14	4.848	0.051	0.0805	0.0004	0.2060	0.0022	2.254	0.029	0.0794	0.0006	0.826	1207	12	1182	14	−2
10.1	448	112	0.25	79	0.000075	0.13	4.857	0.052	0.0797	0.0004	0.2056	0.0022	2.230	0.030	0.0786	0.0006	0.813	1205	12	1163	15	−4

Error in AS3 reference zircon calibration was 0.37% for the analytical session

(e) Summary of SHRIMP U–Pb zircon results for samples SPP 6076

1.1	578	126	0.22	82.6	0.000021	0.04	6.013	0.065	0.0759	0.0004	0.1663	0.0018	1.733	0.021	0.0756	0.0004	0.900	991	10	1084	10	9
2.1	1038	192	0.18	98.7	0.000370	0.62	9.029	0.093	0.0819	0.0004	0.1101	0.0011	1.163	0.019	0.0766	0.0010	0.628	673	7	1111	26	65
3.1	536	106	0.20	79.4	0.000087	0.15	5.804	0.065	0.0775	0.0004	0.1720	0.0019	1.808	0.025	0.0762	0.0006	0.800	1023	11	1101	17	8
4.1	404	71	0.18	49.8	0.000099	0.17	6.964	0.080	0.0773	0.0005	0.1433	0.0016	1.500	0.021	0.0759	0.0006	0.805	864	9	1092	17	26
5.1	1077	47	0.04	136.2	0.000009	0.02	6.796	0.069	0.0719	0.0003	0.1471	0.0015	1.457	0.016	0.0718	0.0003	0.920	885	8	980	9	11
6.1	791	103	0.13	82.7	0.000462	0.79	8.218	0.108	0.0802	0.0004	0.1207	0.0016	1.225	0.029	0.0736	0.0014	0.570	735	9	1031	39	40
7.1	738	52	0.07	68.1	0.000482	0.82	9.318	0.095	0.0822	0.0006	0.1064	0.0011	1.106	0.022	0.0753	0.0013	0.513	652	6	1078	35	65
8.1	596	126	0.21	68.8	0.000095	0.16	7.440	0.096	0.0768	0.0005	0.1342	0.0017	1.395	0.022	0.0754	0.0006	0.832	812	10	1079	17	33
9.1	787	195	0.25	113.6	0.000053	0.09	5.949	0.099	0.0769	0.0003	0.1680	0.0028	1.765	0.031	0.0762	0.0004	0.949	1001	16	1100	11	10
10.1	515	95	0.18	79.3	0.000059	0.10	5.580	0.099	0.0766	0.0011	0.1790	0.0032	1.871	0.044	0.0758	0.0012	0.759	1062	17	1090	31	3
11.1	745	132	0.18	116.3	–	<0.01	5.501	0.056	0.0767	0.0003	0.1818	0.0018	1.925	0.021	0.0768	0.0003	0.926	1077	10	1116	8	4

(*continued on next page*)

Table 4 (*continued*)

Grain. spot	U (ppm)	Th (ppm)	Th/U	$^{206}Pb^{*}$ (ppm)	$^{204}Pb/^{206}Pb$	f_{206} %	Total Ratios				Radiogenic Ratios						ρ	Age (Ma)				
							$^{238}U/^{206}Pb$	±	$^{207}Pb/^{206}Pb$	±	$^{206}Pb/^{238}U$	±	$^{207}Pb/^{235}U$	±	$^{207}Pb/^{206}Pb$	±		$^{206}Pb/^{238}U$	±	$^{207}Pb/^{206}Pb$	±	% Disc
12.1	380	101	0.27	55.2	–	<0.01	5.913	0.065	0.0773	0.0005	0.1691	0.0019	1.802	0.022	0.0773	0.0005	0.882	1007	10	1128	12	12
13.1	617	127	0.21	76.6	0.000398	0.67	6.923	0.071	0.0810	0.0007	0.1435	0.0015	1.490	0.029	0.0753	0.0013	0.520	864	8	1078	34	25
14.1	616	130	0.21	92.7	0.000029	0.05	5.711	0.059	0.0771	0.0003	0.1750	0.0018	1.851	0.021	0.0767	0.0004	0.902	1040	10	1113	10	7
16.1	849	205	0.24	102.5	0.000937	1.59	7.116	0.082	0.0872	0.0072	0.1383	0.0020	1.409	0.199	0.0739	0.0104	0.102	835	11	1038	283	24
17.1	538	38	0.07	77.7	0.000025	0.04	5.943	0.061	0.0753	0.0006	0.1682	0.0017	1.738	0.023	0.0750	0.0006	0.782	1002	10	1068	16	7
18.1	367	143	0.39	60.9	–	<0.01	5.174	0.061	0.0767	0.0005	0.1933	0.0023	2.052	0.027	0.0770	0.0005	0.882	1139	12	1121	13	−2
19.1	805	40	0.05	110.9	0.000005	0.01	6.235	0.067	0.0741	0.0003	0.1604	0.0017	1.637	0.019	0.0741	0.0003	0.928	959	10	1043	9	9
20.1	215	66	0.31	23.3	0.000064	0.11	7.939	0.089	0.0774	0.0006	0.1258	0.0014	1.327	0.020	0.0765	0.0008	0.730	764	8	1108	21	45
21.1	1282	587	0.46	173.3	0.000020	0.03	6.354	0.108	0.0749	0.0011	0.1573	0.0027	1.619	0.036	0.0746	0.0011	0.752	942	15	1058	30	12
22.1	425	78	0.18	58.8	0.000073	0.12	6.208	0.065	0.0772	0.0005	0.1609	0.0017	1.691	0.022	0.0762	0.0006	0.808	962	9	1101	15	14
23.1	895	97	0.11	137.2	0.000006	0.01	5.602	0.063	0.0743	0.0003	0.1785	0.0020	1.827	0.022	0.0742	0.0003	0.929	1059	11	1048	9	−1
Error in FC1 reference zircon calibration was 0.95% for the analytical session. For areas younger than ~800 Ma correction for common Pb made using the measured $^{238}U/^{206}Pb$ and $^{207}Pb/^{206}Pb$ ratios																						
(f) Summary of SHRIMP U–Pb zircon results for sample SPP-414A.																						
1.1	1187	33	0.028	171	–	<0.01	5.976	0.062	0.0738	0.0003	0.1673	0.0017	1.705	0.019	0.0739	0.0003	0.934	997	10	1038	8	4
2.1	962	22	0.022	128	–	<0.01	6.449	0.068	0.0737	0.0003	0.1551	0.0016	1.577	0.018	0.0738	0.0003	0.913	929	9	1035	9	10
3.1	624	26	0.042	86	0.000135	0.23	6.237	0.069	0.0749	0.0005	0.1600	0.0018	1.609	0.023	0.0730	0.0007	0.764	957	10	1013	19	6
4.1	933	20	0.022	134	0.000036	0.06	5.983	0.064	0.0735	0.0004	0.1670	0.0018	1.681	0.020	0.0730	0.0004	0.894	996	10	1014	11	2
5.1	863	121	0.140	75	0.001415	2.51	9.912	0.107	0.0901	0.0038	0.0984	0.0012	0.947	0.076	0.0698	0.0056	0.148	605	7	923	164	35
6.1	942	15	0.016	127	0.000292	0.50	6.392	0.068	0.0778	0.0004	0.1557	0.0017	1.580	0.022	0.0736	0.0007	0.768	933	9	1031	18	10
7.1	1133	4	0.004	168	0.000001	<0.01	5.806	0.061	0.0737	0.0003	0.1722	0.0018	1.749	0.020	0.0737	0.0003	0.929	1024	10	1032	8	1
8.1	1196	213	0.178	141	0.000084	0.15	7.292	0.076	0.0714	0.0003	0.1369	0.0014	1.326	0.016	0.0702	0.0004	0.877	827	8	934	12	11
9.1	930	59	0.063	131	0.000046	0.08	6.087	0.064	0.0736	0.0003	0.1642	0.0017	1.651	0.020	0.0730	0.0004	0.879	980	10	1013	12	3
10.1	925	62	0.067	134	0.000058	0.10	5.913	0.062	0.0737	0.0005	0.1690	0.0018	1.697	0.023	0.0729	0.0006	0.781	1006	10	1010	17	0
11.1	793	41	0.052	109	0.000078	0.13	6.277	0.074	0.0746	0.0004	0.1591	0.0019	1.612	0.022	0.0735	0.0005	0.876	952	10	1028	13	7
12.1	1438	145	0.101	159	0.000405	0.71	7.778	0.084	0.0783	0.0005	0.1277	0.0014	1.276	0.021	0.0725	0.0009	0.659	775	8	1000	25	23
13.1	1115	130	0.116	96	0.000480	0.85	9.968	0.105	0.0785	0.0004	0.0995	0.0010	0.982	0.015	0.0716	0.0008	0.670	611	6	974	24	37
14.1	1112	721	0.648	126	0.002386	4.17	7.569	0.080	0.1079	0.0019	0.1266	0.0015	1.289	0.065	0.0739	0.0036	0.230	768	8	1038	98	26
15.1	1041	7	0.007	160	0.000009	0.01	5.578	0.068	0.0739	0.0006	0.1792	0.0022	1.822	0.026	0.0737	0.0006	0.837	1063	12	1034	16	−3
16.1	696	66	0.095	97	0.000106	0.18	6.161	0.066	0.0738	0.0004	0.1620	0.0017	1.615	0.021	0.0723	0.0005	0.829	968	10	994	15	3
16.2	497	28	0.056	71	0.000065	0.11	6.033	0.066	0.0751	0.0005	0.1656	0.0018	1.694	0.023	0.0742	0.0006	0.820	988	10	1047	15	6
17.1	1439	155	0.108	166	0.000176	0.31	7.435	0.077	0.0729	0.0003	0.1341	0.0014	1.302	0.017	0.0704	0.0006	0.790	811	8	940	17	14
18.1	1001	54	0.054	128	0.000064	0.11	6.743	0.071	0.0732	0.0004	0.1481	0.0016	1.476	0.018	0.0722	0.0005	0.852	891	9	993	13	10
(g) Summary of SHRIMP U–Pb zircon results for sample ULLU2100																						
1999 SHRIMP II																						
1.1 lw	175	88	0.50	30	0.000019	0.03	5.063	0.060	0.0781	0.0007	0.1975	0.0023	2.118	0.032	0.0778	0.0007	0.784	1162	13	1142	19	−2
2.1 lw	119	101	0.85	8	0.000898	1.67	12.159	0.162	0.0610	0.0011	0.0810	0.0013	0.543	0.051	0.0486	0.0040	0.743	502	8			
3.1 lr	388	95	0.25	42	0.000281	0.48	7.877	0.089	0.0753	0.0007	0.1263	0.0014	1.241	0.032	0.0713	0.0016	0.447	767	8	965	47	21
4.1 lw	241	109	0.45	17	–	<0.01	12.497	0.148	0.0590	0.0008	0.0801	0.0010	0.666	0.015	0.0602	0.0012	0.516	497	6	612	43	19
5.1 lr	114	32	0.28	18	0.000399	0.68	5.589	0.071	0.0768	0.0009	0.1780	0.0024	1.774	0.051	0.0723	0.0015	0.753	1056	13	994	42	−6
6.1 lr	730	107	0.15	120	0.000097	0.16	5.250	0.056	0.0765	0.0004	0.1906	0.0021	2.017	0.030	0.0768	0.0005	0.905	1124	11	1115	13	−1
7.1 lr	215	30	0.14	33	0.000215	0.37	5.583	0.064	0.0758	0.0006	0.1786	0.0021	1.808	0.033	0.0734	0.0008	0.818	1059	11	1025	22	−3
8.1 lr	285	76	0.27	44	0.000170	0.29	5.543	0.062	0.0781	0.0006	0.1799	0.0020	1.878	0.036	0.0757	0.0012	0.585	1066	11	1087	31	2
9.1 dc	1388	184	0.13	223	0.000006	0.01	5.349	0.055	0.0760	0.0002	0.1869	0.0019	1.957	0.021	0.0759	0.0002	0.960	1105	10	1093	6	−1
10.1 dc	4938	614	0.12	918	0.000074	0.12	4.623	0.047	0.0772	0.0001	0.2161	0.0022	2.268	0.024	0.0761	0.0002	0.978	1261	12	1099	4	−15
11.1 lw	462	143	0.31	79	0.000025	0.04	5.018	0.054	0.0779	0.0004	0.1992	0.0021	2.130	0.027	0.0775	0.0005	0.852	1171	11	1135	13	−3
2008 SHRIMP RG																						
6.2 lc	287	126	0.44	49	0.000011	0.02	4.999	0.057	0.0813	0.0005	0.2000	0.0023	2.238	0.029	0.0812	0.0005	0.869	1175	12	1226	13	4
6.3 lr	943	162	0.17	158	0.000034	0.06	5.119	0.067	0.0761	0.0003	0.1954	0.0026	2.048	0.038	0.0760	0.0006	0.926	1150	14	1096	16	−5
7.2 lr	419	85	0.20	63	0.000047	0.08	5.712	0.063	0.0755	0.0004	0.1749	0.0019	1.805	0.023	0.0749	0.0005	0.872	1039	11	1065	13	2
7.3 lc	120	40	0.33	21	0.000044	0.07	4.984	0.066	0.0830	0.0008	0.2005	0.0026	2.278	0.041	0.0824	0.0010	0.732	1178	14	1255	24	6
12.1 lr	183	54	0.30	28	0.000118	0.20	5.526	0.066	0.0760	0.0007	0.1806	0.0022	1.850	0.030	0.0743	0.0008	0.729	1070	12	1050	23	−2

13.1 lw	159	47	0.30	27	0.000140	0.24	5.083	0.062	0.0784	0.0006	0.1963	0.0025	2.074	0.052	0.0766	0.0013	0.799	1155	14	1111	33	−4			
14.1 lw	149	46	0.31	25	0.000114	0.19	5.130	0.064	0.0790	0.0007	0.1945	0.0024	2.077	0.036	0.0774	0.0009	0.715	1146	13	1132	24	−1			
15.1 lw	125	53	0.42	20	0.000080	0.13	5.272	0.068	0.0784	0.0008	0.1894	0.0024	2.017	0.038	0.0772	0.0010	0.695	1118	13	1127	27	1			
16.1 lw	151	54	0.36	26	0.000015	0.03	5.038	0.063	0.0790	0.0007	0.1984	0.0025	2.157	0.033	0.0788	0.0007	0.811	1167	13	1167	18	0			
17.1 lw	149	71	0.47	24	–	<0.01	5.410	0.068	0.0775	0.0007	0.1848	0.0023	1.977	0.031	0.0776	0.0007	0.811	1093	13	1136	18	4			
18.1 lr	402	53	0.13	61	0.000288	0.49	5.671	0.063	0.0760	0.0006	0.1762	0.0020	1.825	0.032	0.0752	0.0008	0.800	1046	11	1073	22	2			
18.2 dc	784	318	0.41	116	0.000025	0.04	5.815	0.061	0.0739	0.0003	0.1719	0.0018	1.743	0.020	0.0736	0.0003	0.919	1022	10	1029	9	1			
19.1w	579	134	0.23	85	0.000022	0.04	5.862	0.063	0.0747	0.0004	0.1705	0.0018	1.749	0.021	0.0744	0.0004	0.898	1015	10	1052	11	4			

CL types: lw = light whole grain, lr = light rim, lc = light core, dc = dark core
Error in AS3 reference zircon calibration was 0.37% for the 1999 analytical session
Error in Temora reference zircon calibration was 1.18% for the 2008 analytical session

General Notes and references:
1. Uncertainties given at the one σ level.
2. f206 % denotes the percentage of ^{206}Pb that is common Pb.
3. f206 % denotes the percentage of ^{206}Pb that is common Pb.
4. For % Disc., 0% denotes a concordant analysis.
5. AS3/FC1: Paces and Miller (1993).
6. Temora: Black et al. (2003).

that the igneous intrusion occurred close to peak metamorphic conditions as observed elsewhere.

MAZ12072, Sierra de Maz (29°18′ 15.9″, 68°21′ 37.7″). This rock is an alkali-calcic, high-K, meta-quartz monzonitic orthogneiss (Fig. 4). The main mineralogy is Kfs–Pl–Qtz–Bt–Grt, with accessory Ap, Zr, Ttn, Op, and All. The rock shows a mylonitic fabric, with Kfs porphyroclasts surrounded by a mantle of recrystallized feldspar, polycrystalline quartz ribbons and lepidoblastic biotite aggregates. The fabric suggests a medium-grade metamorphism (Grt–Bt) developed during ductile deformation in a shear zone, affecting a protolith of porphyritic granite or subvolcanic porphyries.

The zircons from this sample range from relatively small, equant anhedral grains to elongate subhedral forms with subround terminations, ranging up to 500 μm in length. The larger grains tend to have irregular grain boundaries and rare grains have central cavities consistent with the entrapment of vapour phases during rapid crystallisation in a volcanic setting. The CL images show either a dominant simple oscillatory zoning or a mixture of this and broad more homogeneous internal structure, the latter common in volcanic zircon grains. Some grains have thin metamorphic overgrowths, and this gives rise to the irregular grains shapes noted above.

The areas analysed do not yield a simple well-grouped cluster on the Wetherill plot, such as that seen in sample MAZ12020. Rather, there is some dispersion in both $^{207}Pb/^{206}Pb$ and $^{206}Pb/^{238}U$ ages (Fig. 12b). The U contents range from ca. 60 to ca. 525 ppm, most being between 60 and 130 ppm; Th/U ratios are in the normal range for igneous zircon. Despite the low U content, the radiogenic $^{207}Pb/^{206}Pb$ ratios and ages are moderately well defined, but the probability density plot highlights some dispersion and tailing on the younger-age side of the dominant age group. This is probably a consequence of the high-grade metamorphic overprint, leading to modification of the original igneous zircon and giving rise to some radiogenic Pb loss and thin newly-formed metamorphic zircon. Notwithstanding this dispersion, a weighted mean for 21 of the 23 analyses reported in the Table gives 1086 ± 10 Ma (MSWD = 1.2) and this provides an estimate for the time of zoned igneous zircon crystallisation.

SPP2067, Sierra de Pie de Palo (31°29′ 12.0″, 68°10′ 51.0″). This is a subalkaline, calcic, metagabbro-diorite (Fig. 8). The main mineralogy is Hbl–Pl–Bt ± Kfs ± Qtz–Czo, Ttn–Zrn, with accessory Ttn and Zrn. The fabric is dominated by porphyroblasts of pale green clino-amphiboles and brown–orange biotites set in a fine granoblastic fabric of Pl, Qtz and Czo. The separated zircons are tabular prismatic grains, mostly with broken terminations and fragments of grains commonly seen in zircons from gabbroic rocks. The grains are usually dark in colour and some have central cavities consistent with trapping of vapour phases during rapid crystallisation. The CL images show a fairly simple internal structure of dominantly length–parallel zonation consistent with a simple igneous origin. U contents are quite high (mostly >300 ppm) giving rise to well-defined radiogenic $^{207}Pb/^{206}Pb$ ratios and ages in the SHRIMP analyses at ca. 1 Ga; Th/U ratios are relatively uniform around 0.20–0.25. All 10 grains analysed yield coincident and concordant U–Pb data (Fig. 12c) and a Concordia age of 1196 ± 8 Ma (MSWD = 1.6). This is significantly older than the two orthogneiss samples from Sierra de Maz and indicates an older period of gabbroic zircon crystallisation.

SPP6076, Sierra de Pie de Palo (31°14′ 06″, 68°05′18″). This is a calc-alkaline mylonitic orthogneiss of granodioritic composition (Fig. 8); its main mineralogy is Kfs–Qtz–Pl–Bt–Ms, with accessory Ep, Zrn, Ap, and Op. The rock displays a conspicuous mylonitic fabric with σ-type Kfs porphyroclasts, fish-type muscovite and euhedral epidote, surrounded by a recrystallized matrix of biotite and quartz.

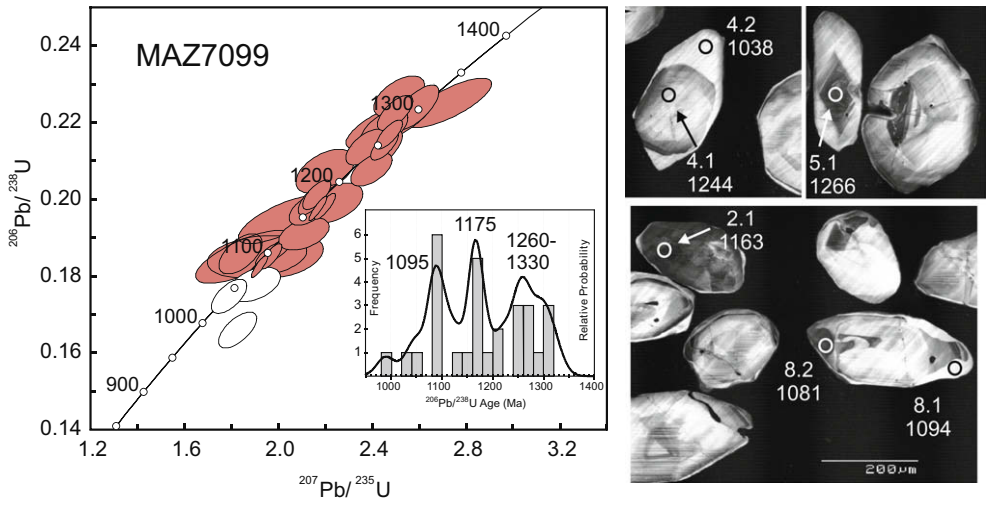

Fig. 11. (a) Wetherill Concordia plot of SHRIMP U–Pb zircon data for orthogneiss sample MAZ7099, (b) typical cathodo-luminescence image for MAZ7099, showing relict igneous cores with broad mantles and occasional outer rims developed during metamorphism. Analysed areas and the determined ages (Ma, shown without errors) are identified (Table 4). See text for detailed interpretation.

The zircons from this sample are equant to elongate grains, subhedral to euhedral, most with sub-round terminations, or are fragments of such grains. They are notably smaller than grains in the other samples, being generally ⩽100 μm in length. The CL images show a range of internal structures. Most have oscillatory zoning, or length–parallel zones consistent with an igneous paragenesis. However, many have a two-part internal structure with either bright CL zoned centres and darker CL zoned outer or rim components. Some grains have an outermost rim or zone with dark, more homogeneous CL. The areas analysed have relatively high U contents, ranging from ca. 215 to ca. 1280 ppm, mostly more than 500 ppm U. Th/U ratios are generally in the range ca. 0.1–0.45 with several grains having ratios ⩽0.07; grains 5 and 19 being the lowest at 0.04 and 0.05, respectively. On a standard Wetherill Concordia plot (Fig. 12d) the data range from concordant within uncertainty to ca. 65% discordant. Note that the analysis of grain 16 is very imprecise and is not considered in this discussion, nor plotted on Fig. 12d. Nineteen of the remaining 22 analyses define a simple Pb loss discordia line with an upper intercept at 1110 ± 10 Ma (MSWD 1.4). The lower Concordia intercept for this line at ca. 77 Ma, albeit with a very large uncertainty, could reflect Andean reactivation but is not relevant to the Grenville-age history. Three analyses plot to the younger-age side of the dominant discordia regression line and it is notable that two of these have the lowest Th/U ratios (grains 5 and 19). The third analysis (grain 23) also has a low Th/U ratio of 0.11, but there are no distinguishing morphological or CL features to indicate that these three analysed areas are otherwise different from those within uncertainty of the dominant Pb loss discordia line. The three analyses scatter about a line that has an upper intercept at about 1055 Ma (MSWD 6.7, not shown on Fig. 12d). The upper Concordia intercept for zoned igneous zircon at 1110 ± 10 Ma is considered to be the best estimate of the protolith age, with indications that a younger metamorphic overprint has given rise to non-zero age radiogenic Pb loss.

SPP414a, Sierra de Pie de Palo (31°18′ 40.0″, 69°55′ 45.0″). This (Fig. 8) from the imbricate thrust domain belongs to an orthogneiss suite that yielded a Rb–Sr whole-rock isochron age of 1021 ± 12 Ma (Pankhurst and Rapela, 1998); it was analysed on SHRIMP as a further control and comparison with the other more recent samples. The main mineralogy is Pl–Qtz–Kfs–Bt–Anf–Grt1–Grt2; accessories are All, Ep, Ap, and Zrn and the metamorphic assemblage is Grt2–Bt–Anf. The granular texture is dominated relict crystals of plagioclase and granular quartz. Two different types of garnet are recognized: Grt1 (igneous?) which is larger, subhedral and devoid of inclusions, and Grt2 (metamorphic), smaller, poikilitic and euhedral, and associated with Bt and Anf.

The zircons from this sample are dominantly metamict elongate, subhedral grains. They are mostly are dark and clouded with alteration products, but a few grains are clear, or there are clear areas on the tips to otherwise metamict zircon. The CL images reinforce the metamict nature of most of the zircon; the few clear areas have weak zoning, but most are dark and featureless. U contents are high, ranging from ca. 500 to ca. 1440 ppm, mostly greater than 900 ppm U. Th contents vary widely, with the Th/U ratio ranging from ca. 0.004 to ca. 0.65; most are <0.07 suggesting that the zircon areas analysed are of a metamorphic origin. As may be expected from the analyses of such metamict and U-rich zircons, most of the analyses are discordant (up to ca. 35%), although 13 are only 10% discordant or less. A regression line fitted to all 19 areas analysed has excess scatter (MSWD = 3.2) with an upper Concordia intercept at 1027 ± 17 Ma (Fig. 12e). The lower Concordia intercept of 166 ± 94 Ma is of doubtful geological significance. A weighted mean of $^{207}Pb/^{206}Pb$ ages for the least discordant group gives 1025 ± 10 Ma (MSWD = 1.7). This is in agreement with the published Rb–Sr age, but is significantly younger than any other Grenville-age event so far determined from the Western Sierras Pampeanas (see Fig. 13). On the basis of the CL images and Th/U ratios it is likely that this reflects a period of metamorphic zircon growth, although it must be noted that the metamict nature of the grains indicates that even the more concordant of analyses may have lost radiogenic Pb during a late Grenville-age fluid movement or thermal episode.

ULLU2100, Precordillera (37°28′ 34.01″; 68°49′ 27.07″). This sample is of a metamorphic xenolith within a Miocene diorite intruded through the Precordillera sequence and cropping out at Ullún, as described by Abruzzi et al. (1993) and Kay et al. (1996). The sample is a calc-alkaline – metagabbro (Fig. 8c), and geochemically it corresponds to the mafic amphibolite group described by those authors. Its main mineralogy consists of Pl–Hbl–Cum/Tr–Bt–Qtz, with accessories Ep, Zrn, Op, and quite common alteration to Chl, Ilm, and sericite. The fabric is formed by a coarse-grained equigranular aggregate of Hb, Pl and clusters of fibrous Cum/Tr clino-amphiboles, probably replacing primary Fe–Mg pyroxene.

The zircons from this sample are quite unusual. Under transmitted light there are two distinct types: a relatively clear

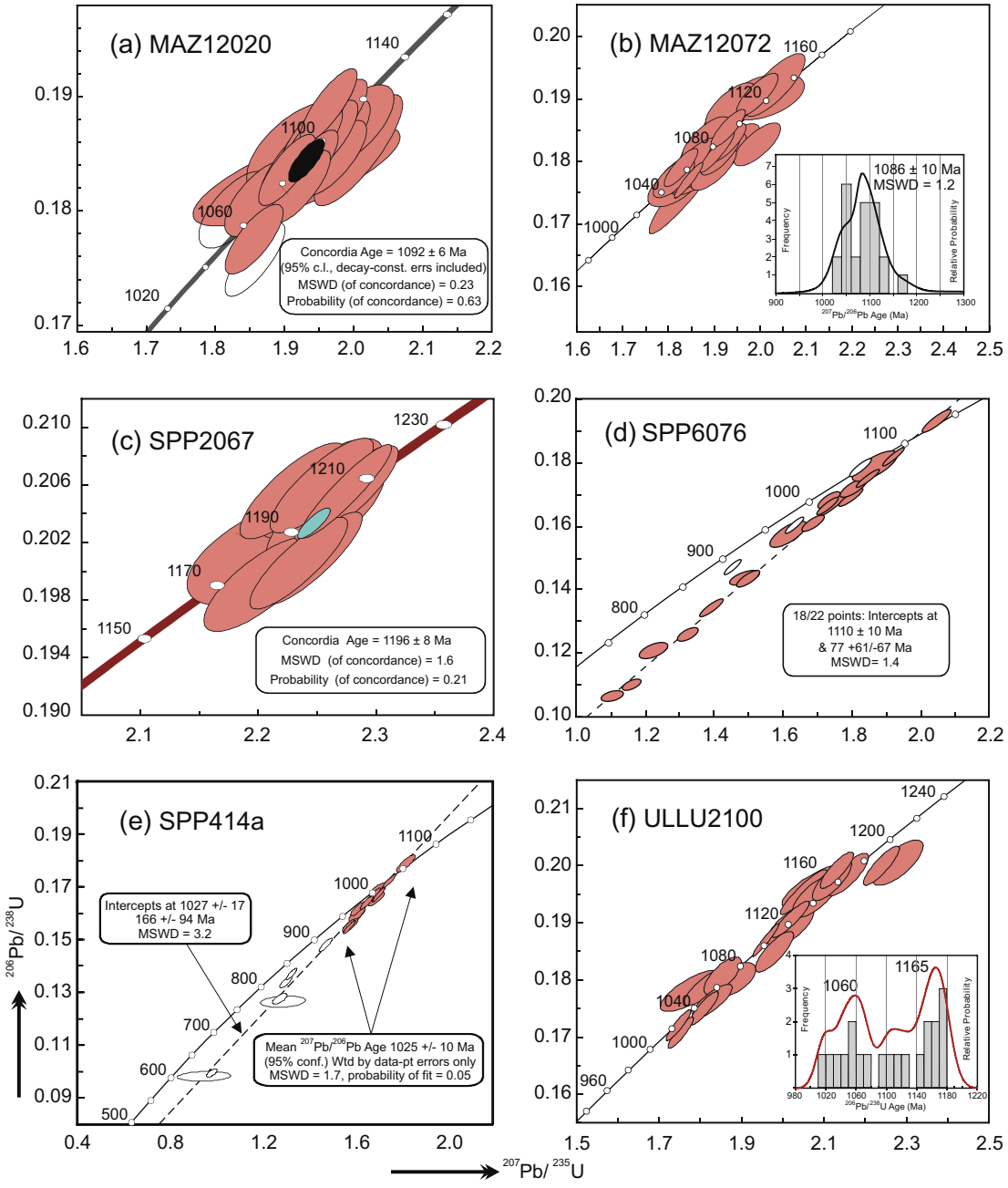

Fig. 12. Wetherill Concordia plots of SHRIMP U–Pb zircon analyses of gneiss samples from Sierra de Maz (a–c), Sierra de Pie de Palo (d and e) and the Ullún xenolith locality in the Precordillera (f). See text for detailed descriptions and interpretation.

anhedral component that forms discrete, larger elongate to sub-equant grains, and a component that is inclusion-rich, in places metamict. The inclusion-rich zircon occurs as elongate to sub-equant, smaller grains that have round to sub-round grain shapes. In places, the clear component can be seen to rim the other. The CL images highlight these markedly different zircon types. The clear zircon is seen as very bright luminescent rims and whole grains. The inclusion-rich component has mottled and very irregular darker CL characteristics, often rimmed by the bright CL component. In some large grains (grains 6 and 7) both rims and cores have bright CL.

The analyses of these complex zircon grains concentrated on the bright CL areas, the dark mottled CL areas being considered metamict and so unlikely to yield consistent or meaningful U–Pb data. Nevertheless, for completeness, some dark mottled CL areas were analysed (see Table 4). Overall there appears to be little correlation between age ($^{207}Pb/^{206}Pb$ or $^{206}Pb/^{238}U$) and spot location, though in general terms the whole clear grains tend to give older ages, greater than 1130 Ma. On the other hand, two clear grains (2 and 4) give Cambro-Ordovician dates that undoubtedly reflect the late history of the Precordillera terrane. There is also little correlation between grain type or CL characteristics and U content; some light CL rims have >500 ppm U, others <200 ppm U; overall the Th/U ratios are in the range ca. 0.2–0.45, which is normal for igneous zircon. The enlarged Wetherill Concordia plot shown as Fig. 12f excludes the two Palaeozoic grains (2 and 4), the normally discordant analysis of grain 3 and the reversely discordant, dark CL core to grain 10 (metamict). The data on this plot form two distinct groupings that are concordant to within analytical uncertainty and distinguished in the relative probability plot of $^{206}Pb/^{238}U$ ages (shown inset). One group is concordant at about 1165 Ma and

AGE (Ma)	Sierra de Maz	U-Pb ages (Ma) Cryst.	U-Pb ages (Ma) Met.	Sierra de Pie de Palo & Ullún	U-Pb ages (Ma) Cryst.	U-Pb ages (Ma) Met.
1000 -						
				~1.03 Ga: Emplacement of TTG suites	1027±17 (1)	
	~1.09-1.07 Ga: Climax of lithospheric extension, emplacement of AMCG complexes. Exhumation of high-grade terrains	1070±41 (2) 1086±10 (1) 1092±6 (1)	*ca.* 1095 (1)			*ca.* 1060 (1)
1100 -						
				~1.11 Ga: New subduction related acid and basic magmatism	1102±6 (6) 1110±10 (1)	
				~1.17 Ga: Arc-related magmatism	*ca.*1165 (1) 1169±8 (5)	
	~1.23-1.17 Ga: Arc-continent collisions Lihospheric thickening and high-grade metamorphism at the continental edge		*ca.* 1175 (1) *ca.* 1180 (3) *ca.* 1230 (3)	*~1.20 Ga: Arc/back-arc oceanic complex N-MORB and oceanic arc lavas*	1196±8 (1) 1204±5 (5)	
1200 -						
	~1.33-1.26 Ga: Andino-type magmatism Emplacement of cordillera granites in Paleoproterozoic sediments	1330-1260 (1)		*~1.24 Ga: Intraoceanic arc subduction (Las Matras block)*	1244±42 (4)	
1300 -						

Fig. 13. Summary of tectonic and magmatic events that affected the Sierra de Maz and Sierra de Pie de Palo–Ullún sectors of the Western Sierras Pampeanas. U–Pb age references: (1) this study, (2) Casquet et al. (2004), (3) Casquet et al. (2006), (4) Sato et al. (2004), (5) Vujovich et al. (2004), and (6) Kay et al. (1996).

the other at about 1060 Ma, with a further subgroup of two discordant analyses (Fig. 12f) that have similar $^{206}Pb/^{238}U$ ratios to the ca. 1165 Ma group, but with older $^{207}Pb/^{206}Pb$ ratios and ages (the inner light CL cores, analyses 6.2 and 7.3). Whilst it is recognised that these are complex zircons that exhibit atypical CL characteristics and structure and ensuing U–Pb systematics, we suggest that the older grouping at ca. 1165 Ma provides an estimate for zircon crystallisation in the gabbroic protolith of this metamorphic xenolith, whereas the ca. 1060 Ma group reflects a period of zircon growth during metamorphism.

5. Discussion: the geodynamic history of the Western Sierras Pampeanas

A summary of the main lithotectonic elements recognized in the Sierra de Maz and Sierra de Pie de Palo–Ullún sectors of the WSP is shown in Fig. 13, based on U–Pb SHRIMP dating of igneous and metamorphic events obtained in representative samples of the different magmatic series identified in each sector (Figs. 4–12). Due to the very complex structural imbrication and the several overprinted events recorded in the WSP, the scenario depicted in Fig. 13 must be tested in future detailed studies of the WSP.

The oldest igneous event registered in the WSP is represented by suites of dioritic to granitic subalkaline orthogneisses of Sierra de Maz (ca. 1330–1260 Ma, Figs. 4a and 11). These rocks are characteristic of Andean-style I-type granites intruded in a continental crust (see Section 4.1.1). Metasedimentary rocks in the SE sector of the Maz Domain that are likely the country rocks of this series contain 1.7–1.9 Ga detrital zircons, indicating a Late Paleoproterozoic source for the metasedimentary envelope, and early Paleoproterozoic Nd model ages (Casquet et al., 2006, 2008). There is no evidence to constrain the length of time taken by this event. Taking into account that the granitic suite is relatively abundant and that zircon metamorphic overgrowths in the country rocks range from 1180 to 1230 Ma (Casquet et al., 2006), the duration of this first stage of continental-edge magmatism has been tentatively extended to approximately 1230 Ma (Fig. 13).

No similar continental-edge environment has been identified in Sierra de Pie de Palo where, in contrast, the oldest rocks (gabbro SPP2067, 1196 ± 8 Ma, Fig. 12c; Vujovich et al. 2004 reported an age of 1204 ± 8 Ma in similar rocks) show clear geochemical evidence of having formed in an oceanic arc/back-arc environment (Vujovich and Kay, 1998; Vujovich et al., 2004) (see Fig. 9a and b). Fig. 13 shows the arc/back-arc oceanic system of Pie Palo evolving separately from the Andino-type margin inferred for Sierra de Maz. The different composition between the juvenile oceanic Sierra de Pie de Palo and the continental, mature environment of Sierra de Maz, is well depicted by their contrasting Nd isotopic signatures (Fig. 6). The juvenile tonalite–trondhjemites of the Las Matras block, further south (Fig. 1), suggest an oceanic arc at ca. 1244 Ma (Sato et al., 2004), either as an earlier stage of the Pie de Palo system, or as an independent arc (Fig. 13).

An important amphibolite facies metamorphic event affected the metadiorite MAZ7099, and produced an age peak ca. 1175 Ma defined by concordant spots in well-developed metamorphic zircon rims (Fig. 11). Metamorphic rims defining a coeval peak at ca. 1180 Ma and an older one at ca. 1230 Ma were reported in garnet schists and basic granulites within a different sliver of the Maz Central Domain (Casquet et al., 2006). Granulite facies (780 °C, 780 MPa) and a crustal depth of *ca.* 29 km were calculated for this Grenville-age metamorphism (Casquet et al., 2006), which is here ascribed to an arc–continent collision in the Sierra de Maz sector (Fig. 13). After the collision, the early continental-edge of Sierra de Maz became a deformed foreland environment and the site of intraplate continental magmatism. The inferred suture between the continent and the accreted oceanic arc is not exposed, but was probably a weakly sheared zone, reactivated by major transcurrent faults during the Cambrian? Docking of the WSP against the Río de la Plata Craton (Rapela et al., 2007; Casquet et al., 2008c).

No equivalent overprinted coeval metamorphic rims have been so far found in the analysed rocks of the Sierra de Pie de Palo–Ullún sector and the Las Matras block (Sato et al., 2000), suggesting that these arc and arc/back-arc systems were not directly involved in the Maz arc–continent collision. What is so far found at ca. 1170 Ma in this sector is the evidence of a new convergent event given by (i) 1169 ± 8 Ma tonalite/granodiorite sills and dykes intruded into the basic arc/back-arc sequence of Sierra de Pie de Palo (Vujovich et al., 2004) and (ii) basic arc magmatism in the Precord-

illera (ULLU2100, ca. 1165 Ma, Fig. 12f, 13). Oceanic arc subduction was operating at the time an arc–continent collision occurred in the Maz sector, suggesting either they were two independent arc systems or that the Pie de Palo–Ullún sector is a southern (present coordinates) remnant branch of the same arc system, not affected by the collision. The Ullún sector has been considered as an oceanic arc/back-arc environment near a continental margin (Kay et al. 1996).

A new episode of convergence in the Pie de Palo–Ullún sector is represented by 1110 ± 10 Ma calc-alkaline orthogneisses (SPP6076, Figs. 8b, 12d, 13) and mafic amphibolite xenoliths (1102 ± 6 Ma, Kay et al., 1996). These ages overlap within errors, and suggest that the Pie de Palo outcrops and the Ullún xenoliths belonged to the same basement at that time. Compared with the previous (ca. 1200 Ma) subduction event of Pie de Palo, the calc-alkaline gneisses show a relatively high La/Yb ratio (Fig. 10), suggesting a plagioclase-poor mineral residue formed in a thicker crust. This event probably affected large sectors of the WSP, taken into account that a suite of 1108 ± 13 Ma calc-alkaline orthogneisses with similar geochemical characteristics (Fig. 10a and b), has been also reported in Sierra de Umango (Varela et al. 2003) (Fig. 10a, b). Altogether the widespread *ca.* 1100 episode suggests that the Pie de Palo–Ullún sector was accreted or adjacent to the continent at that age.

A final Mesoproterozoic subduction event is represented by the 1027 ± 17 Ma Mogote-Corralito tonalite–trondhjemite gneisses (Figs. 12e, 13), which show low $[La/Yb]_N$ between 2.4 and 2.9 (Fig. 9c), indicating a source located above the garnet stability field and therefore within thin crust. An important tectonic event must have taken place between these two younger convergent episodes, to explain their contrasting geochemical signature. Such a significant magmatic event is represented in Sierra de Maz by the 1070–1090 intraplate intrusion of AMCG complexes (Fig. 13). The age of the 1070 ± 41 Ma massif anorthosite of Sierra de Maz (Casquet et al., 2004) overlaps within errors both the 1092 ± 6 Ma meta-mangerite (MAZ12020, Fig. 12a) and the *ca.* 1088 Ma meta-granite (MAZ12072, Fig. 12b) reported here, and interpreted collectively as an AMCG complex. The large uncertainty in the anorthosite age does not allow to confirmation they are truly coeval, but if this interpretation is correct the age of the whole complex would be *ca.* 1090 Ma, i.e., the age of the more precisely dated meta-mangerite. Intrusion of these slightly contaminated mantle-derived magmas during a widespread extensional episode would have produced an important thermal overprint in surrounding rocks. The 1330–1260 Ma meta-granitic suite located close to the AMCG complex (see Fig. 2) shows a peak age of zircon mantle overgrowths at 1095 Ma (Fig. 11). The mafic granulite xenoliths of the Precordillera show zircon metamorphic overgrowths at *ca.* 1060 Ma (Fig. 12f), and the 1102 ± 6 Ma mafic amphibolite xenolith contains two zircon fractions with significantly lower U and Pb concentration, interpreted as a metamorphic event at ~1083 Ma (Kay et al., 1996). This evidence points to a regional thermal event that we here relate to the ponding of mantle magmas at the base of the crust and the intrusion of AMCG complexes during an extensional episode (Fig. 13). Intramontane basins most probably formed during this episode, and should therefore contain only pre-1060 Ma detrital zircons, as is the case of the Morteritos schists in Sierra de El Gigante (Rapela et al., 2007).

Despite the structurally complex imbrication produced by the Paleozoic and Mesozoic (Andean) orogenies, the inferred major Mesoproterozoic geological events and their timing seem to define a protracted but coherent geodynamic history for the Western Sierras Pampeanas. This started at *ca.* 1330 Ma and ended at *ca.* 1030 Ma with convergent events at a continental margin, and included between these limits the formation of oceanic arc/back-arc complexes, arc–continent collisions, renewed subduction and an intraplate extensional episode with intrusion of AMCG complexes. This is the history of a complex, composite arc system developed facing a long-lived ocean.

Although the issues of provenance of the Western Sierras Pampeanas and their original links with other Grenville-age orogens of the terrane collage are beyond the scope of this work, it is necessary to mention that several of the stages described above have been interpreted as evidence for Laurentian provenance, e.g., the basement of the Precordillera (Kay et al., 1996), the arc/back-arc sequence of Sierra de Pie de Palo (Vujovich and Kay, 1998) and the massif-type anorthosites of the Sierra de Maz Central Domain (Casquet et al., 2004), among others. There is no doubt that several of the geodynamic entities identified in the Western Sierras Pampeanas (Fig. 13) have also been described in the Laurentian Grenville belt, such as Andean calc-alkaline magmatic arcs and coeval back-arc deposits, as well as episodes of extension and intrusion of AMCG complexes, the youngest of which was emplaced at *ca.* 1090–1050 Ma (Rivers, 1997; Corrigan and Hanmer, 1997) and was thus broadly coeval with the Maz AMCG complex (Fig. 13). Nevertheless, as Rodinia reconstruction is still a matter of speculative debate, these comparisons should be taken with caution. For example, an arc–continent collision at *ca.* 1170 Ma and an important metamorphism bracketed at *ca.* 1090–1050 Ma have been identified in the Natal-Namaqua belt of southern Africa (Jacobs et al., 2003 and references therein), which in some reconstruction is placed facing the Grenville orogen. Both of these events are conspicuous features now identified in the Western Sierras Pampeanas.

6. Conclusions

The study of Mesoproterozoic rocks of the sierras of Maz and Pie de Palo reveals a protracted (300 Ma long) geological history. As these terrains represent contrasting crustal environments that sometimes experienced coeval events, it is possible to reconstruct and interpret their episodic evolution. Sierra de Maz seems to have been part of a continental crust throughout this period, starting as a Paleoproterozoic continental margin during Andean type-subduction at least 1330 Ma ago. This margin became a foreland intraplate site after an arc–continent collision, developing high-grade metamorphism at 1230–1170 Ma. During an extensional event defining the culmination of the Mesoproterozoic history in the Maz region, the intrusion of *ca.* 1050–1090, mantle-derived, intraplate AMCG complexes produced a strong thermal overprint on previous continental–arc suites. On the other hand, the Mesoproterozoic sequences of the Sierra de Pie de Palo–Ullún sector are dominated by oceanic arc and back-arc rocks, which were products of a fully developed and active arc system *ca.* 1200 Ma ago. A new subduction event at ~1170 Ma overprinted the old arc/back-arc, while a 1110 Ma episode seems to have been emplaced into crust that had become more mature. Now located at the continental margin, the juvenile accreted terranes underwent later emplacement of subduction-related plutons at 1027 Ma. As in other Grenville-age terrains, the geodynamic history of the Mesoproterozoic WSP is dominated by convergent tectonics, either at continental margins or intra-oceanic arcs, with episodes of arc–continent collisions and emplacement of AMCG complexes during extensional events.

Acknowledgements

Financial support for this paper was provided by Spanish MEC Grants BTE2001-1486 and CGL2005-02065/BTE, Universidad Complutense Grant PR1/05-13291 and Argentine Grants PIP-CONICET 5719 and FONCYT PICT 2006-1009. R.J.P. acknowledges the support of the NERC Isotope Geosciences Laboratory at BGS. We appreciate constructive reviews by A. Nutman and R. Fuck.

References

Abruzzi, J.M., Kay, S.M., Bickford, M.E., 1993. Implications for the nature of the Precordilleran basement from the geochemistry and age of Precambrian xenoliths in Miocene volcanic rocks, San Juan province. In: XII Congreso Geológico Argentino y II Congreso de Exploración de Hidrocarburos, Mendoza, Actas, vol. III, pp. 331–339.

Astini, R., Ramos, V.A., Benedetto, J., Vaccari, N., Cañas, F.L., 1996. La Precordillera: un terreno exótico a Gondwana. In: XIII Congreso Geológico Argentino y III Congreso de Exploración de Hidrocarburos, Actas, vol. 5, pp. 293–324.

Baldo, E., Dahlquist, J., Rapela, C.W., Casquet, C., Pankhurst, R.J., Galindo, C., Fanning, C.M., 2005. Early Ordovician peraluminous magmatism in the Sierra de Pie de Palo, (Western Sierras Pampeanas): geotectonic implications. In: Pankhurst, R.J., Veiga, G.D. (Eds.), International Congress "Gondwana 12", Abstracts Academia Nacional de Ciencias. Argentina, p. 57.

Baldo, E., Casquet, C., Pankhurst, R.J., Galindo, C., Rapela, C.W., Fanning, C.M., Dahlquist, J.A., Murra, J., 2006. Neoproterozoic A-type granitic magmatism in the Western Sierras Pampeanas (Argentina): evidence for Rodinia break-up along a proto-Iapetus rift? Terranova 18, 388–394.

Baldo, D.E.G., Casquet, C., Colombo, F., Pankhurst, R.J., Galindo, C., Rapela, C.W., Dahlquist, J., Fanning, C.M., 2008. Magmatismo anorogénico Neoproterozoico (845 Ma) en las Sierras Pampeanas Occidentales de Maz y Umango. Nueva evidencia del rifting temprano de Rodinia? In: XVII Congreso Geológico Argentino, Tomo I, 181p.

Basei, M., Ramos, V.A., Vujovich, G.I., Poma, S., 1998. El basamento metamórfico de la Cordillera Frontal de Mendoza: nuevos datos geocronológicos e isotópicos. In: X Congreso Latinoamericano de Geología y VI Congreso Nacional de Geología Económica (Buenos Aires), Actas, vol. 2, pp. 412–417.

Black, L.P., Kamo, S.L., Allen, C.M., Aleinikoff, J.N., Davis, D.W., Korsch, R.J., Foudoulis, C., 2003. TEMORA 1: a new zircon standard for Phanerozoic U–Pb geochronology. Chemical Geology 200, 155–170.

Caminos, R., 1979. Sierras Pampeanas Noroccidentales. Salta, Tucumán, Catamarca, La Rioja y San Juan. In: Segundo Simposio de Geología, Regional Argentina, Academia Nacional de Ciencias de Córdoba, vol. 1, pp. 225–291.

Casquet, C., Baldo, E., Pankhurst, R.J., Rapela, C.W., Galindo, C., Fanning, C.M., Saavedra, J., 2001. Involvement of the Argentine Precordillera Terrane in the Famatinian mobile belt: Geochronological (U–Pb SHRIMP) and metamorphic evidence from the Sierra de Pie de Palo. Geology 29, 703–706.

Casquet, C., Rapela, C.W., Pankhurst, R.J., Galindo, C., Dahlquist, J., Baldo, E.G., Saavedra, J., González Casado, J.M., Fanning, C.M., 2004. Grenvillian massif-type anorthosites in the Sierras Pampeanas. Journal of the Geological Society, London 162, 9–12.

Casquet, C., Pankhurst, R.J., Rapela, C.W., Fanning, C.M., Galindo, C., Baldo, E., González-Casado, J.M., Dahlquist, J.M., Saavedra, J., 2005. The Maz suspect terrane: a new Proterozoic domain in the Western Sierras Pampeanas. In: Pankhurst, R.J., Veiga, G.D. (Eds.), International Congress "Gondwana 12". Academia Nacional de Ciencias, Argentina, Abstracts, p. 92.

Casquet, C., Pankhurst, R.J., Fanning, C.M., Baldo, E., Galindo, C., Rapela, C., González-Casado, J.M., Dahlquist, J.A., 2006. U–Pb SHRIMP zircon dating of Grenvillian metamorphism in Western Sierras Pampeanas (Argentina): correlation with the Arequipa Antofalla craton and constraints on the extent of the Precordillera Terrane. Gondwana Research 9, 524–529.

Casquet, C., Pankhurst, R.J., Rapela, C.W., Galindo, C., Fanning, C.M., Chiaradia, M., Baldo, E., González-Casado, J.M., Dahlquist, J.A., 2008a. The Mesoproterozoic Maz terrane in the Western Sierras Pampeanas, Argentina, equivalent to the Arequipa–Antofalla block of southern Peru? Implications for West Gondwana margin evolution. Gondwana Research 13, 163–175.

Casquet, C., Pankhurst, R.J., Galindo, C., Rapela, C.W., Fanning, C.M., Baldo, E., Dahlquist, J., González Casado, J.M., Colombo, F., 2008b. A deformed alkaline igneous rock – carbonatite complex from the Western Sierras Pampeanas, Argentina: evidence for late Neoproterozoic opening of the Clymene Ocean? Precambrian Research 165, 205–220.

Casquet, C., Rapela, C.W., Baldo, E., Pankhurst, R.J., Dahlquist, J., González-Casado, J.M., Galindo, C., Fanning, C.M., Saavedra, J., 2008c. Allochthoneity of the Argentine precordillera terrane: an alternative to current paleogeographical models. In: 33th. International Geological Congress, Oslo. CD-ROOM, 1pp.

Cingolani, C.A., Varela, R., 1999. Rb–Sr isotope age of basement rocks of the San Rafael Block, Mendoza, Argentina. In: II South American Symposium on Isotope Geology, Actas, Villa Carlos Paz, Argentina, pp. 23–26.

Corrigan, D., Hanmer, S., 1997. Anorthosites and related terranes in the Grenville orogen: A product of convective thinning of the lithosphere? Geology 25, 61–64.

Eby, G.N., 1990. The A-type granites: a review of their occurrence and chemical characteristics and speculations on their petrogenesis. Lithos 26, 115–134.

Emslie, R.F., 1978. Anorthosite massifs, rapakivi granites, and late Proterozoic rifting of North America. Precambrian Research 7, 61–98.

Ewart, A., 1982. The mineralogy and petrology of Tertiary–Recent orogenic volcanic rocks: with special references to the andesite-basalt compositional range. In: Thorpe, R.S. (Ed.), Andesites. New York, Wiley, pp. 25–95.

Finney, S., 2008. The Cambrian to Carboniferous migration of the Cuyania terrane of western Argentina. In: 33th. International Geological Congress, Oslo. CD-ROOM, 1pp.

Frost, B.R., Barnes, C.G., Collins, W.J., Arculus, R.J., Ellis, S.J., Frost, C.D., 2001. A geochemical classification for granitic rocks. Journal of Petrology 42, 2033–2048.

Galindo, C., Casquet, C., Rapela, C., Pankhurst, R.J., Baldo, E., Saavedra, J., 2004. Sr, C and O isotope geochemistry and stratigraphy of Precambrian and Lower Paleozoic carbonate sequences from the Western Sierras Pampeanas of Argentina: tectonic implications. Precambrian Research 131, 55–71.

Goodge, J.W., Fanning, C.M., Bennett, V.C., 2001. U–Pb evidence of 1.7 Ga crustal tectonism during the Nimrod Orogeny in the Transantarctic Mountains, Antarctica: implications for Proterozoic plate reconstructions. Precambrian Research 112, 261–288.

Hervé, F., Pankhurst, R.J., Fanning, C.M., Calderón, M., Yaxley, G.M., 2007. The South Patagonian batholith: 150 my of granite magmatism on a static plate margin. Lithos 97, 373–394.

Jacobs, J., Bauer, W., Fanning, C.M., 2003. New age constraints for Grenville-age metamorphism in western central Dronning Maud Land (East Antarctica), and implications for the palaeogeography of Kalahari in Rodinia. International Journal of Earth Sciences 92, 301–315.

Kay, S.M., Orrell, S., Abruzzi, J.M., 1996. Zircon and whole-rock Nd–Pb isotopic evidence for a Grenville age and Laurentian origin for the basement of the Precordillera in Argentina. Journal of Geology 104, 637–648.

Kretz, R., 1983. Symbols for rock-forming minerals. American Mineralogist 68, 277–279.

Leat, P.T., Jackson, S.E., Thorpe, R.S., Stillman, C.J., 1986. Geochemistry of bimodal basalt-subalkaline/peralkaline rhyolite provinces within the Southern British Caledonides. Journal of the Geological Society, London 143, 259–273.

Le Maitre, R.W. (Ed.), 1989. A Classification of Igneous Rocks and Glossary of Terms. Recommendations of the International Union of Geological Sciences on the Systematics of Igneous Rocks. Blackwell, Oxford, p. 193.

Leveratto, M.A., 1968. Geología de la zona al oeste de Ullún-Zonda, borde oriental de la Precordillera de San Juan, eruptividad subvolcánica y estructura. Revista Asociación Geológica Argentina 23, 129–157.

Lucassen, F., Becchio, R., 2003. Timing of high-grade metamorphism: early Palaeozoic U–Pb formation ages of titanite indicate long-standing high-T conditions at the western margin of Gondwana (Argentina, 26–29°S). Journal of Metamorphic Geology 21, 649–662.

Ludwig, K.R., 2001. SQUID 1.02, A User's Manual; Berkeley Geochronology Center Special Publication. No. 2, 2455 Ridge Road, Berkeley, CA 94709, USA.

Ludwig, K.R. 2003. User's manual for Isoplot/Ex, Version 3.0, A geochronological toolkit for Microsoft Excel. Berkeley Geochronology Center Special Publication No. 4, 2455 Ridge Road, Berkeley CA 94709, USA.

McDonough, M.R., Ramos, V.A., Isachsen, C.E., Bowring, S.A., Vujovich, G.I., 1993. Edades preliminares de circones del basamento de la Sierra de Pie de Palo, Sierras Pampeanas occidentales de San Juán: sus implicancias para el supercontinente proterozoico de Rodinia. In: XII Congreso Geológico Argentino y II Congreso de Exploración de Hidrocarburos, Mendoza, Actas, vol. 3, pp. 340–342.

Middlemost, E.A.K., 1997. Magmas, rocks and planetary development. Longman, Singapore. 299 pp.

Mulcahy, S.R., Roeske, S.M., McClelland, W.C., Nomade, S., Renne, P.R., 2007. Cambrian initiation of the Las Pirquitas thrust of the western Sierras Pampeanas, Argentina: implications for the tectonic evolution of the proto-Anean margin of South America. Geology 35, 443–446.

Nakamura, N., 1974. Determination of REE, Ba, Fe, Mg, Na and K in carbonaceous and ordinary chondrites. Geochimica et Cosmochimica Acta 38, 757–773.

Paces, J.B., Miller, J.D., 1993. Precise U–Pb ages of Duluth complex and related mafic intrusions, northeastern Minnesota: geochronological insights to physical, petrogenetic, paleomagnetic, and tectonomagmatic process associated with the 1.1 Ga Midcontinent Rift System. Journal of Geophysical Research 98, 13.997–14.013.

Pankhurst, R.J., Rapela, C.W., 1998. The proto-Andean margin of Gondwana: an introduction. In: Pankhurst, R.J., Rapela, C.W. (Eds.), The Proto–Andean Margin of Gondwana, vol. 142. Geological Society, London, pp. 1–9 (special publication).

Pearce, J.A., Harris, N.B.W., Tindle, A.G., 1984. Trace element discrimination diagrams for the tectonic interpretation of granitic rocks. Journal of Petrology 25, 956–983.

Porcher, C.C., Fernandes, L.A.D., Vujovich, G.I., Chernicoff, C.J., 2004. Thermobarometry, Sm/Nd ages and geophysical evidence for the location of the suture zone between Cuyania and Pampia terranes. Gondwana Research 7, 1057–1076.

Ramos, V.A., Vujovich, G., Dallmeyer, R.D., 1996. Los klippes y ventanas tectónicas preándicas de la Sierra de Pie de Palo (San Juan): Edad e implicaciones tectónicas. In: XIII Congreso Geológico Argentino y III Congreso de Exploración de Hidrocarburos, Actas, vol. 5, pp. 377–391.

Ramos, V.A., Basei, M., 1997. The basement of Chilenia: an exotic continental terrane to Gondwana during the early Paleozoic. In: Bradshaw, J.D., Weaver, S.D. (Eds.), Terrane dynamics-97. International Conference on Terrane Geology, Christchurch, New Zealand, Conference Abstracts, pp. 140–143.

Rapela, C.W., Pankhurst, R.J., Casquet, C., Fanning, C.M., Galindo, C., Baldo, E., 2005. Datación U–Pb SHRIMP de circones detríticos en para-anfibolitas neoproterozoicas de la secuencia Difunta Correa (Sierras Pampeanas Occidentales, Argentina). Geogaceta 38, 227–230.

Rapela, C.W., Pankhurst, R.J., Casquet, C., Fanning, C.M., Baldo, E.G., González-Casado, J.M., Galindo, C., Dahlquist, J., 2007. The Río de la Plata craton and the assembly of SW Gondwana. Earth Science Reviews 8, 49–82.

Rivers, T., 1997. Lithotectonic elements of the Grenville Province: review and tectonic implications. Precambrian Research 86, 117–154.

Sambridge, M.S., Compston, W.J., 1994. Mixture modeling of multi-component data sets with application to ion-probe zircon ages. Earth and Planetary Science Letters 128, 373–390.

Sato, A.M., Tickyj, H., Llambías, E.J., Sato, K., 2000. The Las Matras tonalitic–trondhjemitic pluton, central Argentina: Grenvillian-age constraints, geochemical characteristics, and regional implications. Journal of South American Earth Sciences 13, 587–610.

Sato, A.M., Tickyj, H., Llambías, Basei, M.A., González, P.D., 2004. The Las Matras Block, central Argentina (37°S–67°W): the southernmost Cuyania terrane and its relationship with the Famatinian orogeny. Gondwana Research 7, 1077–1087.

Sun, S.-S., McDonough, W.F., 1989. Chemical and isotopic systematics of oceanic basalts: implication for mantle compositions and processes. In: Saunders, A.D., Norry, M.J. (Eds.), Magmatism in the Ocean Basins, vol. 42. Geological Society, London, pp. 313–345 (special publication).

Thomas, W.A., Astini, R., 2008. The Ordovician Ocloyic orogenic belt along western Gondwana. In: 33th International Geological Congress, Oslo. CD-ROOM, 1pp.

Varela, R., Dalla Salda, L.H., 1993. Geocronología Rb–Sr de metamorfitas y granitoides del tercio sur de la Sierra de Pie de Palo, San Juan, Argentina. Revista Asociación Geológica Argentina 47, 271–275.

Varela, R., Valencio, S.A., Ramos, A.M., Sato, K., González, P.D., Panarello, H.O., Roverano, D.R., 2001. Isotopic strontium, carbon and oxygen study on Neorproterozoic marbles from sierra de Umango, Andean Foreland, Argentina. In: III South American Symposium on Isotope Geology, Pucón Chile, Revista Comunicaciones, vol. 52. Santiago, p. 121.

Varela, R., Basei, M., Sato, A., Siga Jr, O., 2003. Proterozoico medio y Paleozoico inferior de la sierra de Umango, antepaís andino (29 S), Argentina: edades U–Pb y caracterizaciones isotópicas. Revista Geológica de Chile 30, 265–284.

Vujovich, G.I., Kay, S.M., 1998. A Laurentian? Grenville-age oceanic arc/back-arc terrane in the Sierra de Pie de Palo, Western Sierras Pampeanas, Argentina. In: Pankhurst, R.J., Rapela, C.W. (Eds.), The Proto–Andean Margin of Gondwana, vol. 142. Geological Society, London, pp. 59–179 (special publication).

Vujovich, G.I., Van Staal, C.R., Davis, W., 2004. Age constraints and the tectonic evolution and provenance of the Pie de Palo Complex, Cuyania composite terrane, and the Famatinian orogeny in the Sierra de Pie de Palo, San Juan, Argentina. Gondwana Research 7, 1041–1056.

Whalen, J.B., Currie, K.L., Chappell, B.W., 1987. A-type granites: geochemical characteristics, discrimination and petrogenesis. Contributions to Mineralogy and Petrology 95, 407–419.

Williams, I.S., 1998. U–Th–Pb Geochronology by ion microprobe. In: McKibben, M.A., Shanks III., W.C., Ridley, W.I. (Eds.), Applications of Microanalytical Techniques to Understanding Mineralizing Processes, Reviews in Economic Geology, vol. 7, pp. 1–35.